공학박사 학위논문

A study on the ionic/electronic hybrid devices for touch sensing and wireless power transfer based on the soft hydrogels

하이드로젤 기반의 터치 센싱과 무선 전력 전송
이온−전자 혼성 장치에 관한 연구

2020 년 2 월

서울대학교 대학원

재료공학부

김 총 찬

A study on the ionic/electronic hybrid devices for touch sensing and wireless power transfer based on soft hydrogels

하이드로젤 기반의 터치 센싱과 무선 전력 전송

이온−전자 혼성 장치에 관한 연구

지도 교수 오 규 환

이 논문을 공학박사 학위논문으로 제출함
2019년 12월

서울대학교 대학원
재료공학부
김 충 찬

김충찬의 공학박사 학위논문을 인준함
2019년 12월

위 원 장 _____ 남 기 태 _____ (인)

부위원장 _____ 오 규 환 _____ (인)

위   원 _____ 선 정 윤 _____ (인)

위   원 _____ 박 철 민 _____ (인)

위   원 _____ 김 도 환 _____ (인)

Abstract

As the rise of ubiquitous computing and the Internet of Thing facilitate the frequent interaction between human and machines, the importance of human machine interfaces (HMI) has been emphasized. Despite recent advances in HMI, current devices based on metals or semiconductors are still limited in use due to mechanical mismatches with humans having soft skins and tissues.

In this respect, hydrogels are promising alternative for conventional conductive materials. The hydrogels are polymer networks swollen with the water. The polymer networks enable the hydrogel to maintain their shape like a solid and to withstand deformation. The water in the hydrogel dissolves the ions, making the hydrogel ionic conductive. Thus, hydrogels with ions can be served as stretchable ionic conductors to transmit electrical signals and power even in the stretched state. However, there are also issues that arise because of the use of ions as charge carriers. Herein, I demonstrate how to solve the issues when using hydrogels and how to take advantage of their characteristics. Two ionic devices were developed and explored; a hydrogel touchpad that can stretch more than 1000% and a gel receiver that can receive electrical power wirelessly.

In first part, highly stretchable and transparent touch panel consisting of hydrogels was explored. Because human-computer interactions are increasingly important, touch panels may require stretchability and biocompatibility in order to allow integration with the human body. However, most touch panels have been developed based on stiff and brittle electrodes. We demonstrate an ionic touch panel based on a polyacrylamide hydrogel containing lithium chloride salts. The panel is soft and stretchable, so it can sustain a large deformation. The panel can freely

transmit light information because the hydrogel is transparent, with 98% transmittance for visible light. A surface-capacitive touch system was adopted to sense a touched position. The panel can be operated under more than 1000% areal strain without sacrificing its functionalities. Epidermal touch panel use on skin was demonstrated by writing words, playing a piano, and playing games.

In second part, we have explored a wireless power transfer system using an ionic conductor as a power receiving parts. A number of implantable biomedical devices that require electric power have been developed and wireless power transfer (WPT) systems are emerging as a way to provide power to these devices without requiring a hardwired connection. Most of WPT have been based on conventional conductive materials, such as metals, which tend to be less biocompatible and stiff. Herein, we describe a development of an ionic wireless power transfer (IWPT) system on the basis of ionic conductor. A power receiver of the IWPT consisting of polyacrylamide hydrogel with NaCl salts was delivered power through the ionic current induced by capacitive coupling. The hydrogel receiver, easy to fabricate, flexible, transparent, and biocompatible, received power at a distance of 5 cm from the transmitter, and even when inserted inside the mouse. Charge accumulation caused by the prevention of discharge on electrical double layers (CAPDE) induced electrochemical reactions in the IWPT. The mechanism of CAPDE was studied and the amount of products was controlled by tuning the circuit parameter.

Keyword: Hydrogels, Ionic conductor, Ionic devices, touch panel, wireless power transfer

Student Number: 2014-30217

Table of Contents

List of Figures

the coupling area of the capacitor. The width of the transmitter was 50 mm. (B) The coupling capacitance was proportional to the width of the gel receiver and the resonance frequency was inversely proportional to the square root of the coupling capacitance. (C) Wide gel receivers delivered more current due to their larger cross-sectional area of the current path.

Fig. 3.10. (A) Maximum current is shown as a function of gap distance with various filling materials. (B and C) With dielectric materials such as air and deionized water, increasing the gap distance resulted in decreased coupling capacitance and increased resonance frequency. However, coupling capacitors filled with NaCl solution maintained a consistent coupling capacitance and resonance frequency regardless of gap distance.

Fig. 3.11. (D) Schematic and an equivalent circuit illustrating a coupling capacitor filled with dielectric materials. CD dominates the capacitance of the circuit and varies with gap distance. (E) Schematic and equivalent circuit illustrating a coupling capacitor filled with electrolyte. R_{bulk} is a variable resistance that changes with gap distance, while $C_D\#1$ and $C_D\#2$ were insensitive to gap distance.

Fig. 3.12. Coupling capacitance and series resistance of the coupling capacitor are shown as a function of electrolyte concentration. The lack of ions in the electrolyte solution increases R_{bulk} and results in decreased power transfer efficiency.

Fig. 3.13. An implantable IWPT device is shown. The gel receivers were encapsulated in polydimethylsiloxane (PDMS). The light-emitting diode

-320 mV) and the counter oxidation reaction (Ag + Cl- → AgCl + e-, E°

= 220 mV) occur at the working electrode (WE) and the counter electrode

(CE), respectively. The products of electrochemical reactions accumulate

at the interface between the gel receiver and the WE.

Chapter 1. Introduction

1.1. Study Background

1.1.1   Ionic conduction

An ionic drift under electric fields is called ionic condcution. Ionic currents in artifical systems can be generated by electric fields while the driving forces for ionic transports in nature are generally gradients of concentration by ion pumps or ion channels. In general, the matrices for ionic systems are available in two phases; one is in solid state and the other is in liquid. In case of solid-state ionics, cermaic compounds like ionic crystals allow displacement of ions [1]. For example, ionic condcution in PbF_2 is activated at 600 K and it becomes higher (450 $\Omega^{-1}\cdot m^{-1}$ at 1000 K) [2]. Liquid-phase matrices like ionic liquids [3] or polar solvents (i.e., water, dimethyl sulfoxide, etc.), on the other hand, support ionic transport at ranges near the room temperature. 1 M potassium chloride solution has specific conductivity of 11.2 $\Omega^{-1}\cdot m^{-1}$ at 298 K [4].

In case of hydrogels with salts, a high portion of solvent molecules imbibed in the gels and the porous structure by polymer networks contribute similar ion-conductive behaviors with liquid-phase conductors [5]. Under the applied voltages, a 100-µm thick polyacrylamide hydrogel containing sodium chloride salts present reasonable sheet resistance ranging from 10^2 to 10^5 $\Omega/\square$ [5]   while 1 to 10^2 $\Omega/\square$ for Ag nanowires with their thickness above 300 µm [6],   20 to 10^4 $\Omega/\square$ for carbon single-wall nano tubes (SWNTs) [7] and 1.6 x 10^3 to 2.5 x 10^5 $\Omega/\square$ for graphene [8]. Based on literatures, ionic conductors including hydrogels and electrolyte solutions can be regarded as comparable charge conductors.

1.1.2   Stretchable ionics.

Stretchable ionic devices have been established by using hydrogels as ionic conductors. Stretchable ionic devices take advantage of hydrogel while compensating the issues on hydrogel, resulting in higher performance than previous studies. A wide variety of devices were built on hydrogels such as sensors, actuators, generators and diodes. These applications have stretchability while performing their original functions. The stretchable applications using ionic conductors present a new vision for stretchable devices.

1.1.2.1 Issues on the stretchable ionic devices

When an electrode is exposed to an electrolyte, electrons in the electrode electrostatically attract ions to maintain charge neutrality. The attracted ions and electrons form a double layer at the interface, referred to as the EDL. The EDL acts as a capacitor and separation between electrons and ions limited to the ion radius enables high levels of capacitance (Fig. 1.1A). The capacitance induced by an EDL forms an imaginary component of the impedance in a circuit. This imaginary component of the impedance makes a phase shift between the current and voltage with time, resulting in a mismatch when not recorded by time. Fig. 1.1B shows a stretchable ionic touch pad that overcomes issues arising from EDL impedance. The ionic touch pad adopts a surface capacitive touch-sensing system. In a typical surface capacitive touch-sensing system, the location of the touching point is determined from induced currents generated from each electrode to the touching point. The induced current is determined from the resistance of a current path, which is proportional to the distance between the electrode and the touching point. However, in an ionic touch pad, the induced current is determined from the impedance rather

2

than from the resistance level. The impedance and distance do not have a proportional relationship due to the imaginary component of the EDL. The impedance is determined from the following equation

$$Z = R - j\frac{1}{2\pi f C_{EDL}} \tag{1.1}$$

where R denotes resistance, f denotes frequency, C_{EDL} is the capacitance of the EDL, and j is an imaginary unit. To suppress the phase shift between the current and voltage, the imaginary component of the impedance should have a smaller value than the real component. By adjusting the resistance of the ionic conductor, the frequency of the AC signal and the capacitance of the interface, $Z \approx R$ is achieved, and the ionic touch pad accurately detects a touching point.

The electrochemical reactions (ECRs) are also an issue to be considered in stretchable ionics. Within a certain range of the potential, referred to as the electrochemical window, the surface of the electrode is polarized without the passage of Faradaic currents at the interface between the electrode and electrolyte (Fig. 1.1C). However, when potentials exceeding the electrochemical window are applied to the interface, charges cross the surface and ECRs occur at the interface. ECRs occurring in ionic devices are typically regarded as side effects of electrode dissolution, gas generation, and oxidation and organic-compound reduction. As high voltages exceeding the electrochemical window are required for some applications, a specialized solution must be employed to prevent ECRs from occurring. An example of a design of a dielectric elastomer actuator without any ECRs is shown in Fig. 1.1D. The dielectric elastomer actuator must achieve high voltages (above 1 kV) to

accomplish actuation. As the applied voltage is much greater than the electrochemical window, an actuator will spur many side effects during operation if it is not specially designed. As is shown in Fig. 1.1D, the structure includes three capacitors arranged in the following sequence: an EDL, a capacitor with a dielectric, and another EDL. Capacitors in this sequence have the same charges at any given moment, $Q = C_{EDL}V_{EDL} = C_{Dielectric}V_{Dielectric}$. As the capacitance of the EDL is much larger than that of the dielectric ($C_{EDL}/C_{Dielectric} \approx 10^7$), the voltage drop occurring through the electrical double layer (V_{EDL}) becomes smaller than the electrochemical window. Typically, 10^{-3} V is dropped through the interface when 10^4 V is applied for actuator use.

1.1.2.2 Applications of stretchable ionic devices

A broad variety of devices have been built based on hydrogels, such as sensors, actuators, generators, and diodes, in consideration of the above issues. These applications are stretchy and perform their original functions. Stretchable applications with ionic conductors are being used in the next generation of stretchable devices.

- Low-Voltage Applications in the Electrochemical Window

Some ionic devices using low voltage with in the electrochemical window have been introduced. Fig. 1.2A shows a stretchable strain sensor using hydrogel [5]. The strain sensor has a capacitor structure consisting of two ionic conductor layers and a dielectric layer stacked alternately. The strain sensor detects motions of a finger after the attachment to the finger. The bending of the finger deforms the strain sensor and increases the capacitance. The strain sensor exhibits good performance, showing a wide strain detection range from 1% to 500%, dynamic durability with cyclic tests,

and linearity. The conformal contact between the strain sensor and skin enhances a sensitivity of the sensor, which enables to detect small and weak strain deformations such as heart beat, stimuli by blood pressure, and vibration of a vocal cord. Fig. 1.2B shows a pressure sensor using hydrogel [9]. The pressure sensor shares the basic operating structure with the previously mentioned strain sensor. The pressure sensor measures changes of the capacitance by external pressure. The pressure sensor can detect a gentle touch of a finger (<10kPa).

Fig. 1.2C and D shows stretchable ionic touch pads for contact and position sensing [10, 11]. A touchpad allows human and devices to interact through a variety of gestures. Fig. 1.2C shows an ionic touch pad based on a surface capacitive touch (SCT) [10]. SCT system detects the touching location through current ratio induced by finger touch. Since SCT-based touch pads are composed of just one conducting layer and four electrodes, their simple structure enhances a durability of the touch pad during a large deformation. The touch pad shows perfect operation even at 1000% of areal expansion and can be operated on complex curved surfaces such as skins, keeping its conformal contact with the skin. Projected capacitive touch sensing (PCT) which is frequently used as a touch pad in mobile device is another sensing system for ionic touch pads (Fig. 1.2D) [11]. The ionic touch pad using PCT has cross-grid arrays of ionic conductor. The grids in row and column will generate capacitive coupling, and the touch pad measures the change of coupling. Since each combination of row and column is measured independently, it is possible to detect multi-touch.

- High voltage applications beyond the electrochemical window

As high voltages beyond the electrochemical window become available with the stacked structure, the field of the stretchable devices using hydrogels can be

broaden. A variety of the stretchable device using stacked structure have been developed such as an actuator [5, 12], a loudspeaker [5], a light emitting device [13-15], and a generator [16]. Fig. 1.3A shows a dielectric elastomer actuator with ionic conductors [5]. When a voltage is applied to the dielectric elastomer actuator, the two ionic conductors with oppositely charged ions attract each other. The attraction force causes thickness contraction and areal expansion of the dielectric elastomer actuator. The ionic loudspeaker in Fig. 1.3B is inspired by the dielectric elastomer actuator [5]. The vibrations of the high frequency by actuations generate the sound. The loudspeaker can cover full range of audible frequency of human being, showing that the ionic conductor has enough speed to convert high frequency to mechanical actuations through ionic conductors.

A stretchable light emitting devices have been developed based on ionics (Fig. 1.3C) [14]. The stretchable light emitting devices has a capacitor structure which consists of two layers; one is a transparent ionic condutor layer and the other is a dielectric layer embedding electroluminescent phosphor. ZnS phosphors which are embedded in the dielectric layer emit light through the transparent ionic conductor under an AC electrical field. Because the ionic conductor is highly transparent for visible light, the emitted light can pass through the ionic conductor without loss.

Since most wearable devices require isolated system, wearable power supplys which can make an electric field to ionic devices are essential [16, 17]. Fig. 1.3D shows a stretchable triboelectric nanogenerator converting mechanical movement into electrical enegy by employing the triboelectric effect [17]. When the electrification occur at the surface of the generator, a current in metal wire is electrostatically induced through the ionic conductor. The harvester can be easily mounted on a

6

skin and convert the mechanical energy to electricity by human motions. Notably, the electrical output performance is not decreased even when stretched (strain 800 %) due to the inherent stretchability of hydrogel.

- Applications with electrochemical reactions

Most ionic devices try to avoid electrochemical reactions due to side effects. However, some applications use electrochemical reactions to generate main functions of the devices. Fig. 1.4A shows a structure of an ionic diode with controlled oxidization of liquid metal [18]. Liquid metal, EGaIn, is used as a deformable electrode in the diode and the hydrogel is used as electrolyte. The forward bias allows ion transport and the backward bias inhibits the ionic current owing to the formation of the insulating oxide layer between EGaIn and gel electrolyte. The diode exhibits rectification ratios up to 450 in a range of -5~5V. Fig. 1.4B demonstrates a paper based ionic diode rectifying ionic currents by a precipitation of AgI [19]. The paper-based ionic diode are composed of a $AgNO_3$ containing layer, a porous separator, and a KI containing layer. When the reverse bias is applied to the device, Ag^+ and I^- meet at the interfacial area and form a precipitated AgI. As the ions are consumed by precipitation before reach to the electrodes, the ionic current is suppressed. The rectification performance of the diode reaches 46 when it is bent.
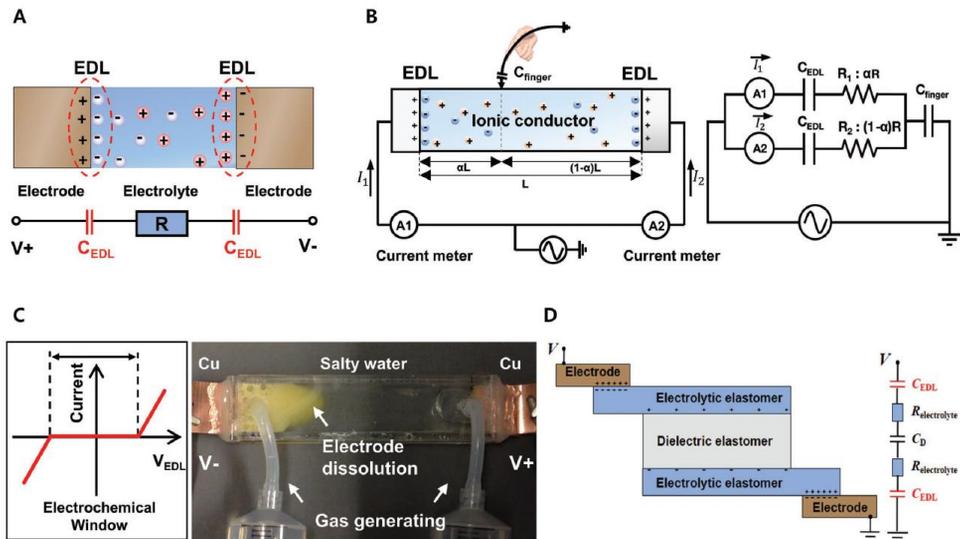
Fig. 1.1. (A) The electrical double layer (EDL) forms at the interface of the electrode and electrolyte. (B) The capacitance of the EDL in the stretchable ionic device increases the impedance of the circuit [10]. (C) Outside of the electrochemical window, electrochemical reactions occur at the interface. (D) In the stacked structure, much of the applied voltage drop occurs in the dielectric capacitor [9].
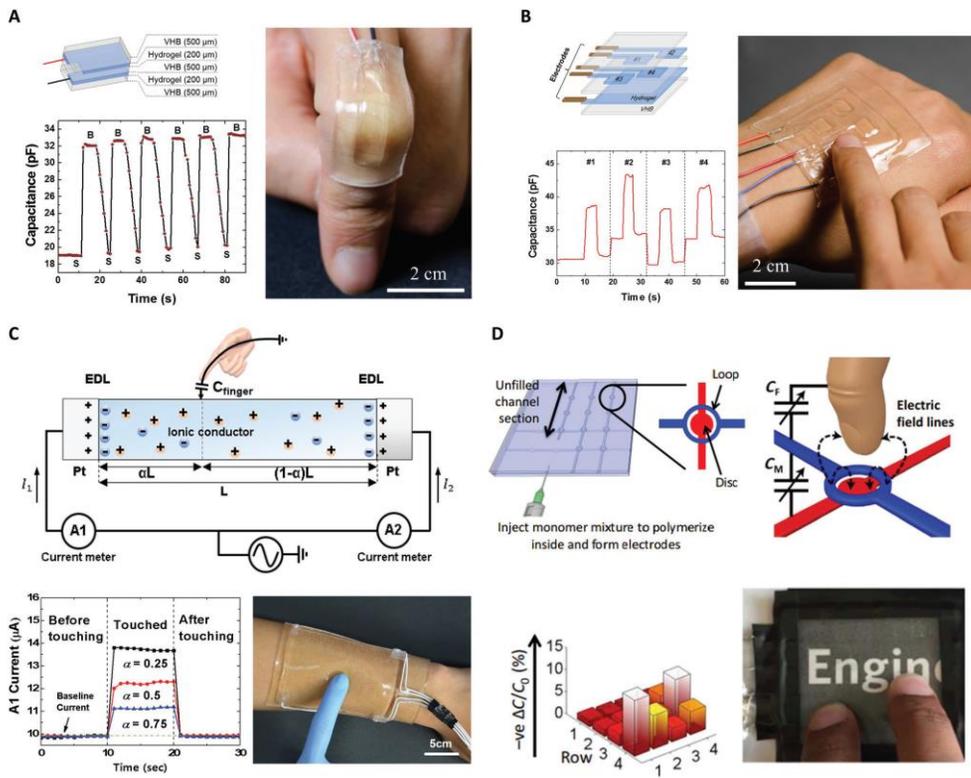
Fig. 1.2. Low-voltage applications in the electrochemical window. (A) A strain sensor based on an ion-containing hydrogel [9]. (B) A capacitor-type pressure sensor based on a hydrogel [9]. (C) A touch pad composed of ionic conductors is employed via a surface capacitive touch-sensing system [10]. (D) An ionic touch pad based on the projected capacitive touching system [11].
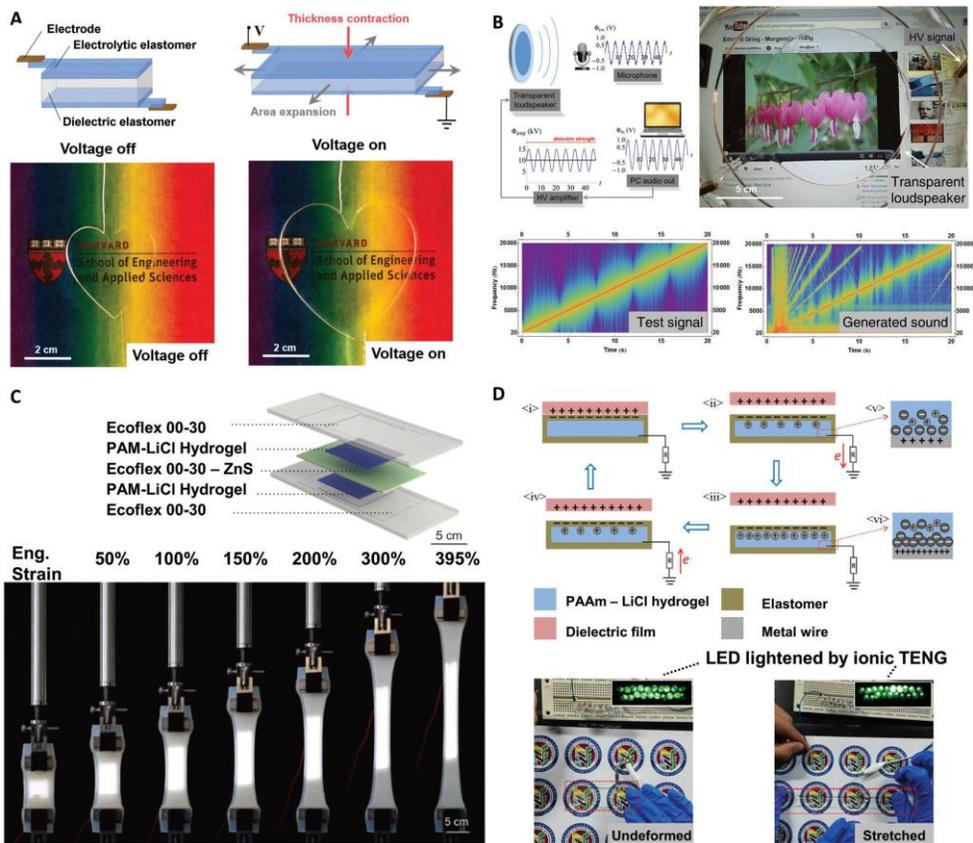
Fig. 1.3. High-voltage applications beyond the electrochemical window. (A) A dielectric elastomer actuator with ionic conductors [5]. (B) An ionic transparent loudspeaker [5]. (C) A stretchable light-emitting device that employs an electroluminescent phosphor [14]. (D) A triboelectric nanogenerator based on ionic conductors [17].
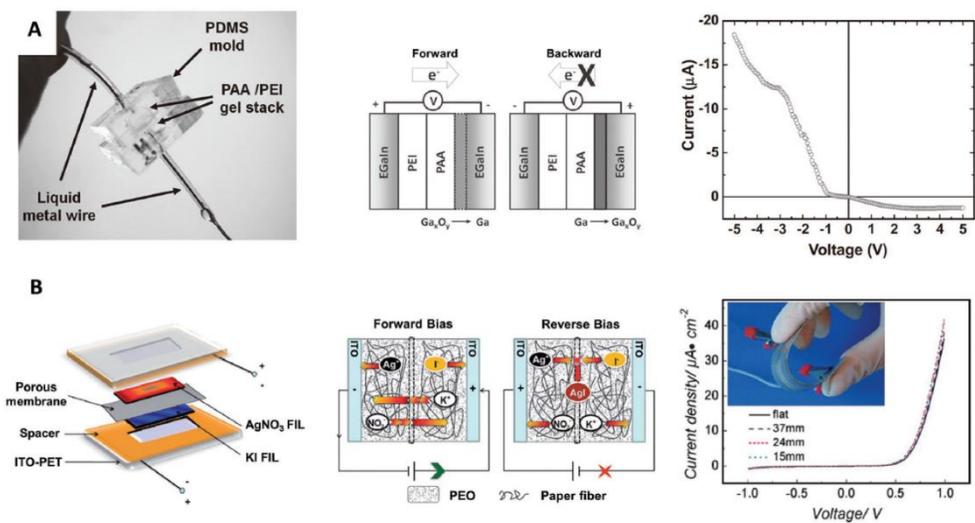
Fig. 1.4. Applications with electrochemical reactions. A) An ionic diode with controlled liquid-metal oxidization. The diode is composed of liquid metal electrodes and gel electrolytes. The formation and reduction of a resistive oxide layer at the interface of the EGaIn and electrolyte leads to asymmetric behavior in the ionic currents [18]. (B) A paper-based ionic diode composed of an AgNO3-filled layer, a separator, and a KI-filled layer. AgI precipitation rectifies ionic currents [19].

1.2. Purpose of Research

This dissertation covers research on ionic devices using hydrogel. The hydrogels are used as an ionic conductor exhibiting high stretchability, transparency and biocompatibility. The dissertation is composed of two parts in large. In the first part, we described highly stretchable ionic touch panel composed of hydrogels including LiCl salts. The ionic touch panel could be stretched 10 times compare to the its own size while maintain their functionality. Because the ionic touch panel can fit into a complex surface like a human skin, an epidermal touch panel was developed, and used for writing words, playing music, and playing games. In the second part, an ionic wireless power transfer system (IWPT) was developed. In IWPT system, an ionic hydrogel acts as a receiver plate for power delivered from a metal transmitter. The characteristics of this system were explored under various conditions. To assess the biocompatibility of our IWPT system, hydrogel receivers were implanted subcutaneously in mice and power was transferred. In addition, the IWPT was used to electrochemically generate NADPH. This study facilitates the development of new biocompatible and functional wireless devices.

Reference

[1]   K. Funke, Solid State Ionics: from Michael Faraday to green energy-the European dimension, *Science and Technology of Advanced Materials* **14**, 50 (2013)

[2]   C. E. Derrington, A. Navrotsky, and M. O'Keeffe, High temperature heat content and diffuse transition of lead fluoride, *Solid State Communications* **18**, 47-49 (1976).

[3]   K. Rajan, A. Chiappone, D. Perrone, S. Bocchini, I. Roppolo, K. Bejtka*, et al.*, Ionic liquid-enhanced soft resistive switching devices *RSC Advances* **6**, 94128-94138 (2016)

[4]   R. A. Bockris J.O., Modern Electrochemistry. v.1 Ionics (2ed., Kluwer) **1** (2002).

[5]   C. Keplinger, J.-Y. Sun, C. C. Foo, P. Rothemund, G. M. Whitesides, and Z. Suo, Stretchable, transparent, ionic conductors, *Science* **341**, 984-987 (2013)

[6]   S. De, T. M. Higgins, P. E. Lyons, E. M. Doherty, P. N. Nirmalraj, W. J. Blau, et al., Silver Nanowire Networks as Flexible, Transparent, Conducting Films: Extremely High DC to Optical Conductivity Ratios, *ACS Nano* **3**, 1767-1774 (2009)

[7]   V. Scardaci, R. Coull, and J. N. Coleman, Very thin transparent, conductive carbon nanotube films on flexible substrates, Applied Physics Letters   **97**, 3 (2010)

[8]   S. De, P. J. King, M. Lotya, A. O'Neill, E. M. Doherty, Y. Hernandez, et al., Flexible, Transparent, Conducting Films of Randomly Stacked Graphene from Surfactant-Stabilized, Oxide-Free Graphene Dispersions, *Small* **6**, 458-464 (2010)

[9]   J. Y. Sun, C. Keplinger, G. M. Whitesides, and Z. G. Suo, Ionic Skin,

Advanced Materials **26**, 7608-7614 (2014)

[10] C. C. Kim, H. H. Lee, K. H. Oh, and J. Y. Sun, Highly stretchable, transparent ionic touch panel, *Science* **353**, 682-687 (2016)

[11] M. S. Sarwar, Y. Dobashi, C. Preston, J. K. M. Wyss, S. Mirabbasi, and J. D. W. Madden, Bend, stretch, and touch: Locating a finger on an actively deformed transparent sensor array, *Science Advances* **3**, 8 (2017)

[12] B. Chen, Y. Bai, F. Xiang, J.-Y. Sun, Y. Mei Chen, H. Wang, et al., Stretchable and transparent hydrogels as soft conductors for dielectric elastomer actuators, *Journal of Polymer Science Part B: Polymer Physics* **52**, 1055-1060 (2014)

[13] J. Wang, C. Yan, G. Cai, M. Cui, A. Lee-Sie Eh, and P. See Lee, Extremely Stretchable Electroluminescent Devices with Ionic Conductors, *Advanced Matererials* **28**, 4490-4496 (2016)

[14] C. Larson, B. Peele, S. Li, S. Robinson, M. Totaro, L. Beccai, et al., Highly stretchable electroluminescent skin for optical signaling and tactile sensing, *Science* **351**, 1071-1074 (2016)

[15] C. H. Yang, B. Chen, J. Zhou, Y. M. Chen, and Z. Suo, Electroluminescence of Giant Stretchability, *Advanced Materials* **28**, 4480-4484 (2016)

[16] W. Xu, L.-B. Huang, M.-C. Wong, L. Chen, G. Bai, and J. Hao, Environmentally Friendly Hydrogel-Based Triboelectric Nanogenerators for Versatile Energy Harvesting and Self-Powered Sensors, *Advanced Energy Materials* **7**, 1601529 (2017)

[17] M. L. Xiong Pu, Xiangyu Chen, Jiangman Sun, Chunhua Du, Yang Zhang, Junyi Zhai, Weiguo Hu, and Zhong Lin Wang, Ultrastretchable, transparent triboelectric nanogenerator as electronic skin for biomechanical energy harvesting and tactile sensing, *Science Advances* **3**, 31 (2017)

[18]   J.-H. So, H.-J. Koo, M. D. Dickey, and O. D. Velev, Ionic Current Rectification in Soft-Matter Diodes with Liquid-Metal Electrodes, *Advanced Functional Materials*, **22**, 625-631 (2012)

[19]   R. Zhao, X. Zhang, J. Xu, Y. Yang, and G. He, Flexible paper-based solid state ionic diodes, RSC Advances **3**, 23178 (2013)

Chapter 2. Highly stretchable, transparent ionic touch panel

2.1. Introduction

Integrated touch panels provide an easy and intuitive interface for interacting with display devices. Panels have been developed with several types of sensing systems including resistive (*1, 2*), capacitive (*3, 4*), surface acoustic wave (*5*), and infrared (*6*) touch. Resistive touch sensing and capacitive touch sensing have become common in electronic devices such as mobile phones, computers, ticketing machines, point-of-sale terminals, and information kiosks (*6, 7*).

Both resistive and capacitive touch sensing require transparent conducting films (TCFs). Indium tin oxide (ITO) has been mostly used owing to its sufficiently low sheet resistance (< 200 Ω/sq) and transparency (*8*). However, because the next generation of touch panels requires stretchability and biocompatibility to allow integration with the human body, touch panels based on ITO face issues owing to their brittle nature. Alternatives such as conducting polymers (*9, 10*), carbon nanotubes (CNTs) (*11, 12*), graphene (*13, 14*), and metal nanowires (*15, 16*) have been investigated for their combination of stretchability along with transmittance for visible light. However, the sheet resistance of these materials sharply increased when they were stretched, and these materials showed fatigue failure when repeatedly stretched (*17*). Furthermore, the bio-compatibility of these alternative materials still must be demonstrated (*18, 19*).

Hydrogels are hydrophilic polymer networks swollen with large amounts of water. Hydrogels are soft like tissue and very stretchable (*20*). Many hydrogels are biocompatible, so they can be used for drug delivery (*21*), tissue replacement (*22*), and wound healing (*23*). Some hydrogels are transparent, allowing for 99 % transmittance for the full range of visible light (*24*), so they can be used to transmit optical information. Because hydrogels contain large amounts of water, which can dissolve ions, they can serve as ionic conductors. Strain sensors, pressure sensors (*25, 26*) and actuators (*24*) have been created with hydrogels as an ionic conductor by stacking conductor/insulator/conductor layers. Thus, hydrogels can be a key ingredient for the next generation of touch panels because of their stretchability, biocompatibility, and transparency. We demonstrate an ionic touch panel using polyacrylamide hydrogel containing LiCl salts.

2.2. Experimental section

2.2.1   Materials

Unless otherwise indicated, the ionic touch panel was built using LiCl-containing polyacrylamide hydrogel as the primary material. Acrylamide (AAm; Sigma, A8887) and lithium chloride (LiCl; sigma, L4408) were used as the base materials of the hydrogel and the ionic charge carrier. N,N-methylenebisacrylamide (MBAA; Sigma, M7279) was used as the cross-linking agent for the AAm gel. Ammonium persulfate (AP; Sigma, A9164) and N,N,N',N'-tetramethylethylenediamine (TEMED; Sigma, T7024) were used as the thermal initiator and accelerator for the gelation reactions, respectively. VHB 4905/4910 (3M) was used as the dielectric elastomer. A Pt electrode and Cu wire were used for the electrical circuit.

The ionic hydrogel was synthesized by dissolving AAm monomer powder and LiCl in deionized water. The molar concentrations of AAm and LiCl aqueous solutions were 2.17 M and 2 M throughout the entire experiments, respectively. The cross-linker MBAA 0.06 wt.% and the initiator APS 0.16 wt.%, with respect to the AAM monomer, were added. After sonicating and degassing the mixture in a vacuum chamber, TEMED 0.25 wt.%, with respect to the weight of the AAm monomer, was added as the accelerator. The solutions were poured into polymethylmethacrylate (PMMA) molds with different sizes for touch panels. The gel was prepared after 1 h. In our study, three types of hydrogel touch panel shapes, a strip type, a circular type, and a rectangular type, were built for each case.

2.2.2 An ionic touch strip.

The strip type of the ionic touch sensing system was made for verifying the 1-D case. The ionic touch strip was fabricated with polyacrylamide hydrogel containing 2 M LiCl aqueous solution and Pt wires for electrodes, which prevented electrochemical reactions at the interface between the electronics (electrons in the electrode) and the ionics (electrolytes in the hydrogel) (29). The Pt wires were glued to the touch strip and connected to current meters (Multimeter, Model 34461A, Agilent) located at each side of the touch strip. A function generator (Model 33612A, Agilent) was then connected to two parts of the current meter to apply the same phase of AC currents on both sides of the gel strip. LiCl was used as a charge carrier and a volatilization inhibitor, which allows hydrogels to dry slowly (28).

A strip, 15 cm in length, was characterized to figure out the correlation between the distance from the electrode to the touch point and the current. To demonstrate the relation, the strip was touched, and the current was recorded by current meters at various touch points. The strip was touched by a gloved finger. For the stretched mode, the strip was elongated to two times its original length and held to the substrate. Like the preceding undeformed case, the measured currents were recorded according to the touch points. The AC voltage from the function generator was -0.6 to 0.6 V, and the frequency was varied from 10 to 100 kHz. Because the voltage was maintained below 1 V, electrochemical reactions were prevented (29). During the experiments, the touch strip was washed with deionized water to remove impurities. After washing, the moisture was not removed to make the touch strip easier to handle because the bare and dried ionic touch panel became sticky. In this case, some moisture was helpful to handle and operate the ionic touch panel

19

2.2.3   Transparent ionic touch panel.

The ionic touch panel was polymerized in the acrylic mold, which was designed for each purpose. The thickness of the ionic touch panel was 3 mm, the same as the touch strip. Two types of ionic touch panels were intentionally made; one was rectangular for 2-dimensional demonstration and comparison with the simulation. The other was circular for a biaxial stretching situation.

When the ionic touch panel was first operated with the controller board, the output figure was not fit to a display. The output figure was represented too small or too large, and the center of the input figure did not correspond with the center of the output figure. The manufacturer of the controller board (3M) provided the calibration tool (MT 7 software control panel, version 7.14.4) for optimal accuracy. The ionic touch panel was fit to the display by conducting a 3-point calibration.

2.2.4   Epidermal touch panel.

VHB, (3M) marketed as an adhesive tape, played a role as the insulator for making the epidermal touch panel. The gel panel was fixed on the VHB film, and 4 electrodes were connected to the corners of the touch panel. The completed epidermal touch panel could be attached to human skin without losing its functionalities. The operating voltage and frequency were the same as the 1-D strip and 2-D touch panel. In attached states, the epidermal touch panel was fully transparent, showing human skin under the touch panel, and was successfully operated.The epidermal touch panel can detect motions including tapping, holding, dragging and swiping. The capability to perceive diverse motions in attached states can be a strength when it used in multiple devices with displays or other output devices.

2.3. Results and Discussion

2.3.1   A working principle of an ionic touch strip.

Among the various types of touch sensing systems, a surface capacitive system was adopted for our ionic touch panel. In a surface capacitive touch system, the same voltage is applied to all corners of the panel, which results in a uniform electrostatic field across the panel. When a conductor, such as a human finger, touches the panel, the touch point becomes grounded, and a potential difference is generated between the electrode and the touch point. The potential difference causes current to flow from the electrode through the finger. The magnitude of the current is determined by the distance between the touch point and electrode. As the distance decreases, a larger current is induced (*27*). This system is limited to a single touch, but it is simple in terms of structure because the panel consists of only one conductor layer and only four electrodes, with one at each corner.

Fig. 2.1A shows the architecture of a 1-dimensional ionic touch strip. A strip of polyacrylamide (PAAm) hydrogel containing LiCl salts (2 M) was used as an ionic conductor. The strip was connected to Pt electrodes on both sides, and the same phase AC voltage was applied through current meters A1 and A2 to both ends. When a finger touched the strip, a closed circuit was formed because the finger was grounded, which allowed current to flow from both ends of the strip to the touch point. The signals were detected by current meters at each corner. The corresponding circuit diagram of the ionic touch strip is shown in Fig. 2.1B. The strip is virtually divided into two resistive parts by the touch point. Each resistor was connected with a capacitor of an electrical double layer and a current meter in series; these two parts were connected in parallel. This parallel circuit was connected in series with a

capacitor created by a finger. In the parallel circuit of Fig. 2.1B, the effect of the capacitor that was formed by the electrical double layer was negligible because of the large capacitance of the electrical double layer and high operating frequency. The position of the touch point can be represented by a normalized distance, α. The left end and the right end of the strip correspond to $\alpha = 0$ and $\alpha = 1$, respectively.

The current flowing in two resistors can be represented by the following equations:

$$I_1 \approx \frac{R_2}{R_1+R_2} I_t = (1 - \alpha)I_t \qquad (2.1)$$

$$I_2 \approx \frac{R_1}{R_1+R_2} I_t = \alpha I_t \qquad (2.2)$$

where I_1 and I_2 are the touching currents measured from current meters A1 and A2, respectively, and $I_t = I_1 + I_2$. The derivations of Eq. (2.1) and (2.2) are discussed in chapter 2.3.2. The current change depending on the touch is shown in Fig. 2.2. Baseline currents on the order of micro amperes were detected. The baseline current is a leakage current that flows through the parasitic capacitor formed between the panel and the environments (*30*). When a finger touches the gel strip, additional currents are drawn from the electrode to the finger. Here, we define this induced current as a "touching current". The latency of the touching current was under 20 ms. The touching current was proportional to the proximity of the electrode to the touch point. The strip was touched from the left electrode to the right electrode every 1 cm, and the measured currents from the A1 current meter and A2 current meter are shown in Fig. 2.3A. The sum of I_1 and I_2 remained constant, and I_1 linearly decreased, whereas I_2 increased as the touch point moved to the right. The resolution of the ionic touch strip will be limited by the resolution of the current meter. With a current meter, which has a resolution in the nanoampere range, the strip showed a resolution

on the order of 10^{-4} m (Fig. 2.9.). The gel strip was stretched to two times its initial length ($\lambda=2$, $L=30$ cm). When the gel strip was stretched (Fig. 2.3B), the parasitic capacitance of the strip increased because of the area expansion. Thus, the baseline current and the touching current both increased compared with that of the non-stretched states. In the stretched states, the currents also showed similar negative linear correlations with the interval of the electrode and the touch points.
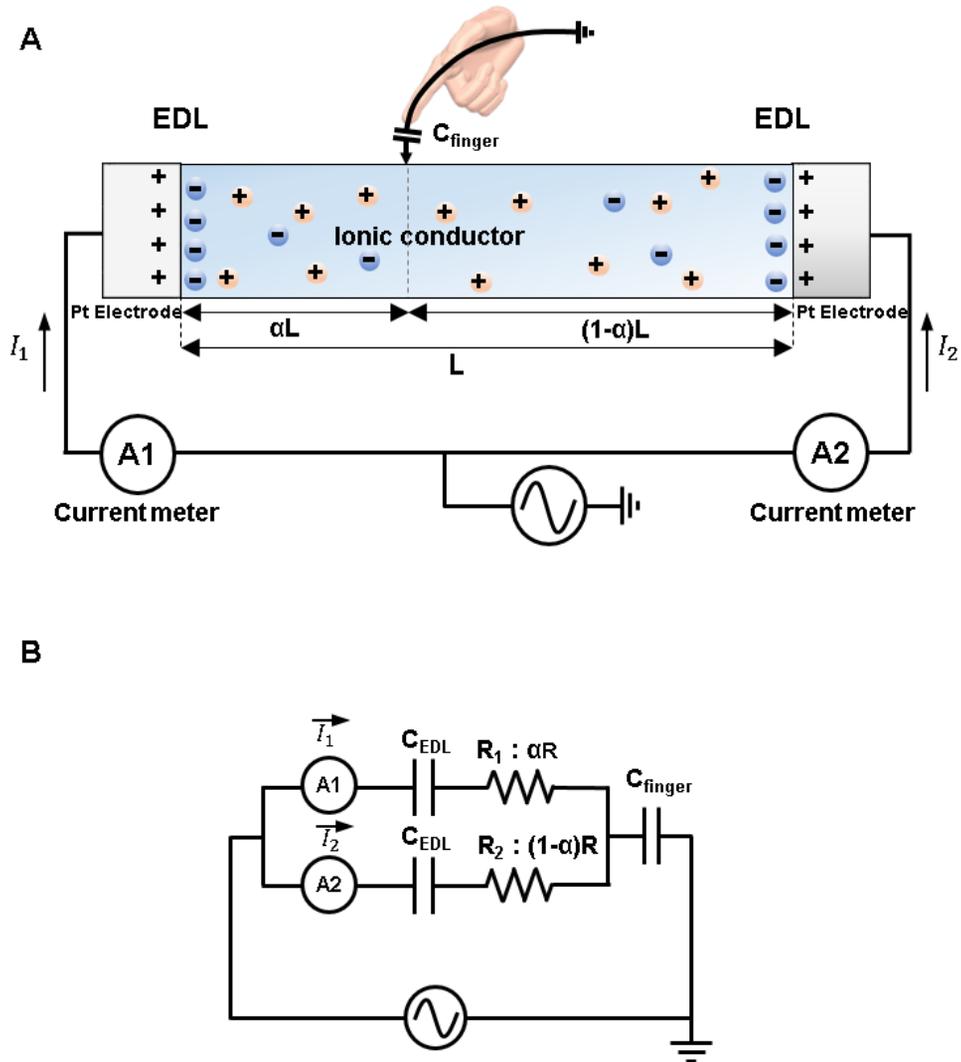
Fig. 2.1 (A) A schematic of a 1D ionic touch strip. When a finger touched the strip, a closed circuit was formed because the finger was grounded, which allowed current to flow from both ends of the strip to the touch point. (B) An electrical circuit diagram of the ionic touch strip.
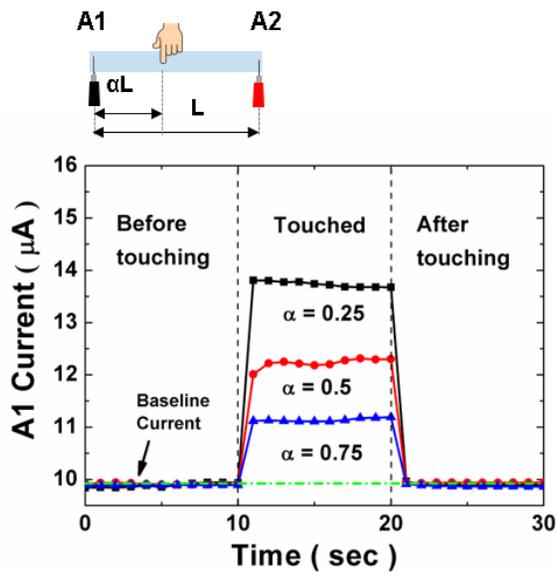
Fig. 2.2 The A1 current was recorded for various touch points (a = 0.25,0.5, and 0.75). Additional touching current flowed when the strip was touched by a finger. The magnitude of the A1 current increased when the touch point became closer to the A1 electrode. The current returned to the baseline value when the strip was no longer being touched.
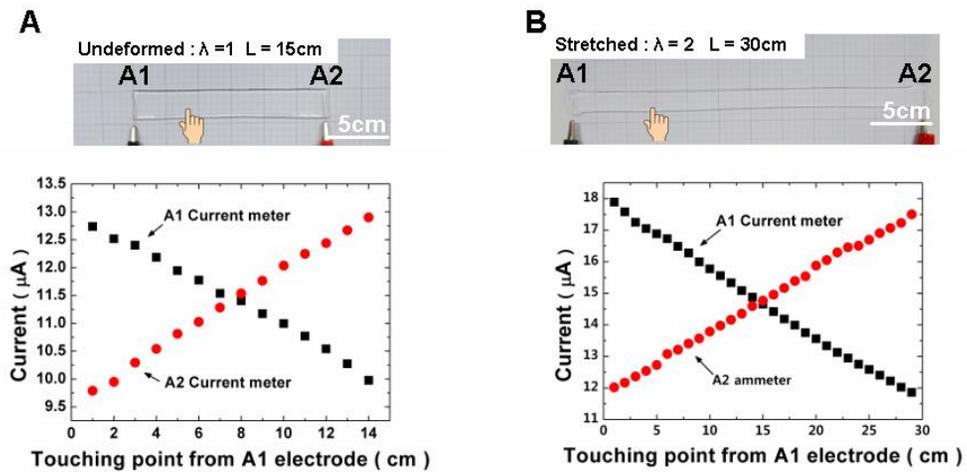
Fig. 2.3. (A) The average currents in a touched period were measured from A1 and A2 according to the distance from the touch point to the A1 electrode. (B) Linear relationship between the distance of the touch point and the current yield was maintained even after a stretching of l = 2.

2.3.2 Sensing mechanism for a 1-dimensional touch strip

We have studied the sensing mechanism of an ionic touch panel with a 1-D strip model. The 1-D model provides a simplified description of a current flowing through the ionic touch sensing system. The model was composed of two resistors and three capacitors as shown in Fig. 2.1.B. When a finger touches the ionic touch strip, current flows from the electrodes to the grounded human finger through the ionic touch panel. The resistances of two resistors were determined by the position of touching.

$$R_1 = \alpha R \tag{2.3}$$

$$R_2 = (1 - \alpha)R \tag{2.4}$$

where R is the total resistance of a strip, and α is a normalized position. Each resistor was connected with a capacitor of an electrical double layer in series. Thus, the impedance (Z) of two paths can be written as

$$Z_1 = R_1 - j\frac{1}{2\pi f C_{EDL}} \quad , \quad Z_2 = R_2 - j \frac{1}{2\pi f C_{EDL}} \tag{2.5}$$

The capacitance per unit area of an electrical double layer (C_{EDL}) was approximately 10^{-1}F/m² (24); the area of the double layer was approximately 10^{-5} m²; and the frequency we have tested was on the order of 17 kHz, so the reactance of the double layer was $-j\frac{1}{2\pi f C} \approx$ -9j. Because the reactance was much smaller than the resistance of the ionic touch strip ($R \approx 200\Omega$), the impedance $Z = 200 \ \Omega - 9j \ \approx 200.2\angle -2.57$ could be approximated by the resistance value ($Z \approx R$). This

approximation allowed the touching current to be calculated by a ratio between two resistances. When a capacitor was added by a finger (C_{finger}) to the circuit in series, the total current flowing through the circuit was

$$I_{\text{total}} = \frac{V}{\frac{R_1 R_2}{R_1 + R_2} - j\frac{1}{2\pi f C_{\text{finger}}}} \tag{2.6}$$

$$I_1 \approx I_{\text{total}} \cdot \frac{R_2}{R_1 + R_2} = (1 - \alpha) I_{\text{total}} \tag{2.7}$$

$$I_2 \approx I_{\text{total}} \cdot \frac{R_1}{R_1 + R_2} = \alpha I_{\text{total}} \tag{2.8}$$

Furthermore, Eqs. (2.6) and (2.8) were rearranged into

$$(1 - \alpha) = \frac{I_1}{I_{\text{total}}} \tag{2.9}$$

$$\alpha = \frac{I_2}{I_{\text{total}}} \tag{2.10}$$

2.3.3   Latency of the ionic touch panel

The latency of the ionic touch panel was determined by analyzing a touching current incurred at the moment of touching. The current was measured using a digital multimeter (Agilent 34461A), which has maximum scan rate of 50 samples per second. As shown in Fig. 2.4, we could not detect any delays from the signal. We suspect that the response time of the touch strip may be less than 20 ms (Fig. 2.4).

The thickness of a gel panel affects the response time of the panel. The thickness is inversely proportional to the resistance. High resistance causes an increase in the RC delay ($\tau = RC$) in a circuit. Because the latency of the touch panel affects the user experience, it is important to determine an adequate thickness of the gel panel. The latency of a gel strip with different thicknesses (0.1 mm, 0.5 mm, 1 mm and 3 mm) was investigated in Fig 2.5. The current was measured using a digital multimeter (Agilent 34461A), which has maximum scan rate of 50 samples per second. However, we could not detect any delays from our ionic touch strip, even with a 0.1 mm thick gel strip, which had highest resistance among them. Instead, we could theoretically calculate the RC delay of the gel strip. The resistance of the 0.1 mm thick gel is approximately 10 k Ω, and the capacitance of the finger is approximately 100 pF (*31*). Therefore, the RC delay in the gel strip is $\sim 10^{-6}$ s, which is much smaller than the minimum interval of sampling in our current meter.
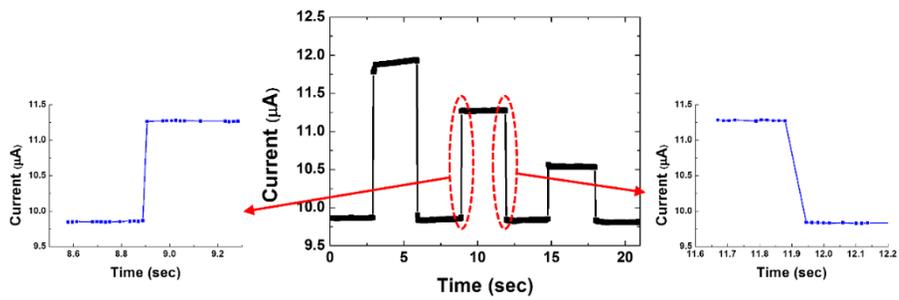
Fig. 2.4. The response time of the ionic touch panel was investigated by determining the latency of a touching current. The current was measured using a digital multimeter (Model 34461A, Agilent), which has maximum scan rate of 50 samples per second. To determine the response time, the graphs were magnified.
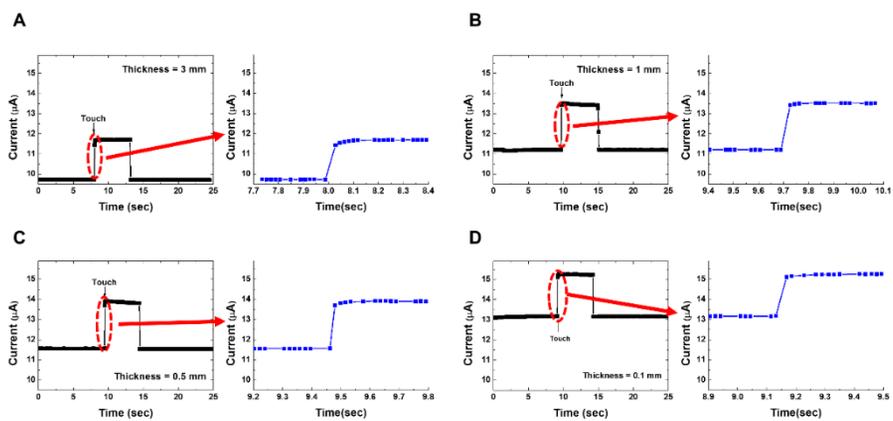
Fig. 2.5. The response time of a gel strip with various thicknesses of (A) 3 mm, (B) 1 mm, (C) 0.5 mm and (D) 0.1 mm.

2.3.4   Parasitic capacitance and baseline current.

When a touch panel is in a steady and untouched state, there should theoretically be no current flow because no electrical potential gradient exists over the panel. However, current flows occur in the steady state owing to parasitic capacitance. Parasitic capacitance is usually formed between environments and a circuit, and leakage current flows to ground through what is called a baseline current (*30*). In our ionic touch panel system, parasitic capacitance seems to exist between the ionic touch panel and environments (Fig. 2.6), which has significant meaning because it determines the baseline current, which is considered as a noise signal. Therefore, the effort to reduce the baseline current was the next subject to improve the performance of the ionic touch panel. The parasitic capacitance of the touch panel was affected by changing the surface area, thickness and resistance as shown Fig. 2.3 and 2.17.
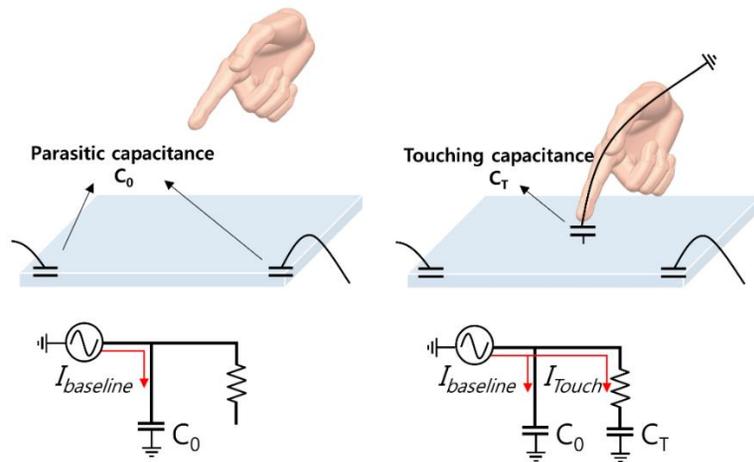
Fig. 2.6. Illustration of the parasitic capacitance and current flow in a capacitive touch panel and the related circuit diagrams.

2.3.5   Accumulated currents induced by touches during the stretching of a gel strip.

We have investigated how stretching and touching affect the current signals flowing through the ionic touch panel. Fig. 2.7 shows the current changes caused by touches during stretching of a gel strip. The gel strip (150 mm × 20 mm × 3 mm) was uniaxially stretched with a strain rate of 0.2/min. Both stretch and touch simultaneously induced a current, but those two factors were differently reflected to a current signal. The touching current was instantly induced when the strip was touched during stretching, which caused a steep slope in the current signal. The baseline current, however, continuously increased according to the strain, which had a relatively gentle slope. By comparing the slope of the current, we can distinguish the current signals separately. Similarly, when the touch panel was stretched equi-biaxially, the baseline current gently increased, but the touching current was instantly induced when the panel was touched. As with the uniaxial stretch, each current signal from stretching and touching can be distinguished by their slope.

Moreover, we suspect that an expansion of the surface area of the gel may cause an increase in the baseline current owing to its increased parasitic capacitance. The surface area of the gel was driven as follows when it was uniaxially stretched.

$$\frac{A}{A_0} = \frac{L_x L_y + L_x L_z + L_y L_z}{l_x l_y + l_x l_z + l_y l_z} = \frac{l_x l_y \sqrt{\lambda_x} + l_x l_z \sqrt{\lambda_x} + {}^{l_y l_z}/{}_{\lambda_x}}{l_x l_y + l_x l_z + l_y l_z} \qquad (2.11)$$

where A_0 and A are surface areas of the gel before and after stretching, respectively. l is the initial length of the gel, and L is the current length of the gel. λ is the stretch in the gel. The subscripts l, L and λ denote a direction of the coordinate axis. We assumed the incompressibility of the materials, $\lambda_x \lambda_y \lambda_z = 1$, and a condition of

34

uniaxial tension, $\lambda_y = \lambda_z = \frac{1}{\sqrt{\lambda_x}}$, was applied. When the dimensions of the sample were length $(l_x) = 150$ mm, width $(l_y) = 20$ mm and thickness $(l_z) = 3$ mm, we typically obtained $A/A_0 = \left(3450\sqrt{\lambda_x} + \frac{60}{\lambda_x}\right)/3510$. The increase in surface area under uniaxial tension is plotted in Fig. 2.7 and compared with the experimentally measured currents. The baseline current showed a similar tendency to the change in surficial area.

2.3.6 Strain rate effects of a gel strip during a uniaxial stretching.

The current signals from a gel strip under various strain rates were investigated for use in dynamic applications. The gel strip was stretched with various strain rates (0.2/min, 0.4/min, 0.6/min and 1/min). As shown in Fig. 2.8, the baseline current shows insensitivity to strain rate in the range of 0.2–1/min.
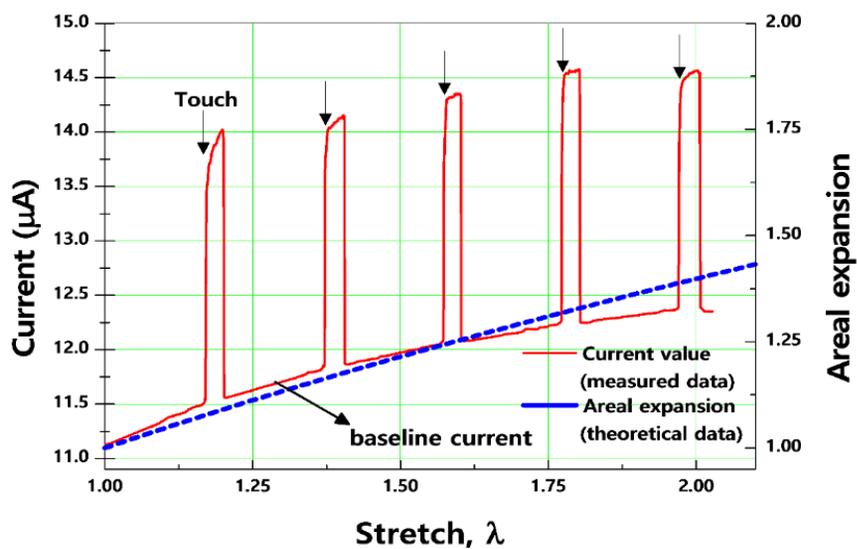
Fig. 2.7. Accumulated currents induced by touch during the stretching of a gel strip. The gel strip (150 mm × 20 mm × 3 mm) was uniaxially stretched with a strain rate of 0.2/min. The baseline current increased during the stretch according to the expansion of the surface area of the gel.
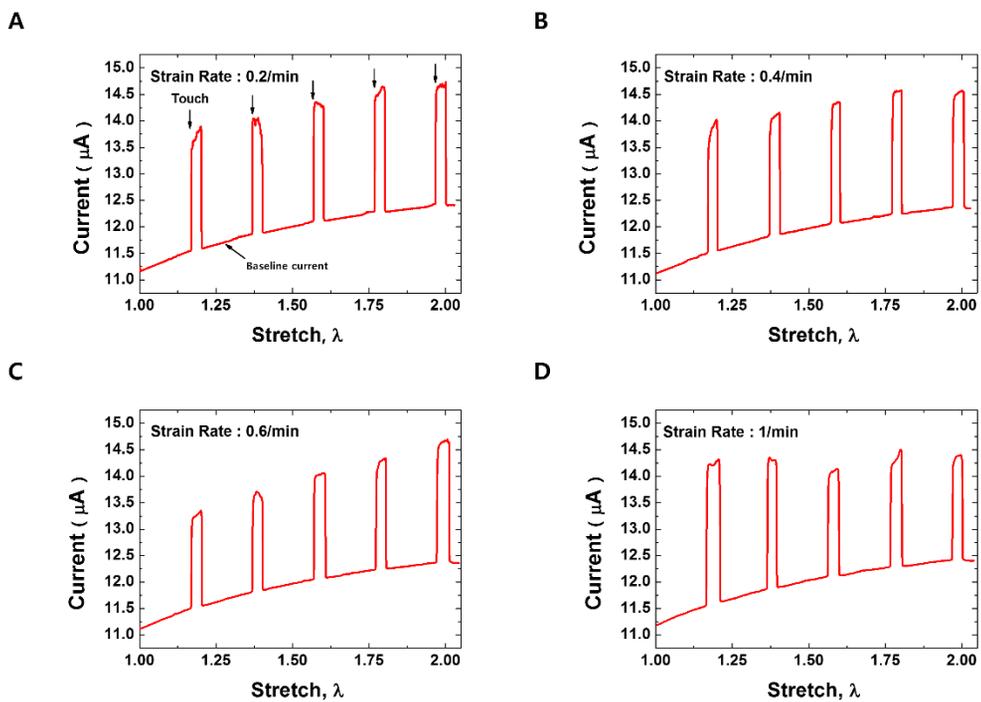
Fig. 2.8. Strain rate effects of a gel strip during a uniaxial stretch. The baseline currents were not influenced by the strain rate during stretching.

2.3.7   Resolution of the ionic touch panel.

High resolution is necessary to develop an accurate and reliable touch panel. Capacitive touch sensing systems have higher resolution than other touch sensing systems such as infrared grid touch and surface acoustic wave touch. There are two types of the capacitive touch sensing systems: projected capacitive touch (PCT), which is typically used for smartphones, and surface capacitive touch (SCT), which is adopted in our ionic touch panel. The PCT panel is made up of a grid pattern of indium tin oxide (ITO), layered on a sheet of glass. It can detect a touch point by measuring the change in the mutual capacitance of grids. The resolution of the PCT is related to the number of grids and the grid interval. Typically, the grid interval is in a range of millimeters, and the controller is used to interpolate the exact touch coordinate at the space between the grids. However, the SCT panel does not have any grids. It has only one layer of continuous conductive material. If the conductive material is homogeneous, the resolution of the SCT panel will be limited by the resolution of the current meter. The current meter used in our experiment has a resolution in the nanoampere range, which corresponds to a touch panel resolution on the order of 10^{-4} m. As displayed in Fig. 2.9, a gel strip was swiped with a finger from one end to the other. The current was continuously recorded from the A1 current meter during the swiping. The current signals were linearly decreased as the distance from the touched point to electrode A1 increased (Fig. 2.9B). A close-up view of the graph is shown in Fig. 2.9C. Approximately ten touch points were detected within 1 mm of swiping, which correspond to a 10^{-4} m resolution.
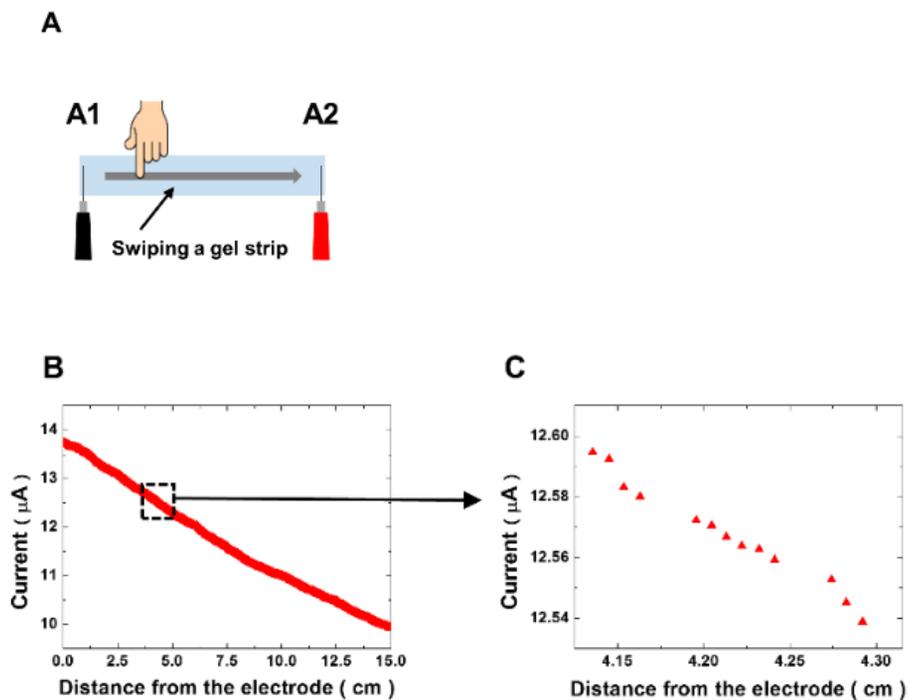
Fig. 2.9. (A) A gel strip was swiped from electrode A1 to electrode A2. A current meter was installed at electrode A1, and the current was continuously recorded with a maximum rate of 50 samples/s during the swiping. The swipe was conducted for 20 s, and more than 1000 touch points were measured. (B) The current decreased linearly in accordance with the position of the touch point. (C) The magnified graph showed that approximately ten touch points were detected within 1 mm of swiping.

2.3.8 Position-sensing in a 2D ionic touch panel.

A 2-dimensional hydrogel panel was tested to detect the position of the touch point. As shown in Figs. 2.10A and 2.11A, a thin hydrogel film, which was rectangular in shape, was connected to the Pt electrodes at each corner. Four current meters were also installed between the voltage source and each corner. Two normalized distances, α and β, were used to indicate the position of the touch on the panel. The lower-left corner of the panel corresponded to $(\alpha, \beta) = (0, 0)$, and the upper right corner corresponded to $(\alpha, \beta) = (1, 1)$. When the panel is touched by a finger, it can be virtually divided into four resistive sections by the touch point (Fig. 2.10B). In the circuit, four virtual resistors are connected together in parallel, and this parallel circuit of resistors is connected to the capacitor by the finger in series. In Fig. 2.11A, the test positions of the touches are displayed. Touch points (TP) TP#1 (0.25, 0.75), TP#2 (0.75, 0.75), TP#3 (0.75, 0.25), and TP#4 (0.25, 0.25) were investigated. These points were sequentially touched, and the current changes were measured from the four current meters installed at each corner. The measured currents from each current meter are plotted in Fig. 2.11B. When TP#1 was touched, the closest current meter, A1, from the touch point showed the largest value, and the farthest current meter, A3, displayed the lowest value. In this two-dimensional case, the touching current gained from the four current meters was proportional to the proximity of the electrode to the touch point, which is similar to the case of the strip. The current values could be used to calculate the coordinate of the touch points in the 2-dimensional panels.

A controller board was designed to help communication between the ionic touch panel and a computer. A block diagram of the board is shown in Fig. 2.12. The board generates a drive voltage signal, and the signal is applied to the corners of the

panel. The board measures the currents to each corner. The currents were on the order of a few microamperes; thus, the currents were amplified and converted to digital form to calculate coordinates of the touch. Because the measured currents and coordinates showed negative linear correlation, the positions were calculated based on following equations (*27*):

$$\alpha \propto \frac{I_2+I_3}{I_1+I_2+I_3+I_4} \tag{2.12}$$

$$\beta \propto \frac{I_1+I_2}{I_1+I_2+I_3+I_4} \tag{2.13}$$

where I_1, I_2, I_3, and I_4 are increased currents by a touch measured at current meters A1, A2, A3, and A4, respectively. As shown in Fig. 2.11B, when a finger touches the same α-coordinate, the value of Eq. (2.12) is determined to be the same. The β-coordinate shows the same tendency as the α-coordinate.

The ionic touch panel was attached to monitor #1, which displayed an input figure (Fig. 2.13). A one-millimeter thick polymethylmethacrylate (PMMA) plate was applied between the panel and the monitor for an electrical insulation. The panel was connected to a computer through the controller board, and the computer displayed an output figure on monitor #2 based on a signal from the controller board. We drew a man on the ionic touch panel. Some distortion was observed on the edge of the output figures. Two concentric squares were drawn through the gel panel to test the distortion. As shown in Fig. 2.14, the outer square showed more distortion than the inner square. To investigate the reason for the distortion, an electrical finite element method simulation was performed. The boundary conditions are displayed in Fig. 2.15A, and the electrical currents that flowed through the four corners were

calculated at various touch points (α, β). A uniform electrical conductivity (1 S/m) was applied over the panel, and the potential of four corners was fixed at 1 V. The panel was split into ten grids in rows and columns. Each intersection of the grids, which is regarded as a touch point, was sequentially grounded (0 V). $(I_1 + I_2)/(I_1+I_2 + I_3 + I_4)$ and $(I_2 + I_3)/(I_1+I_2 + I_3 + I_4)$ for each touch point are plotted in Fig. 2.15B and C, respectively. As shown in Fig. 2.15B, the contour lines near the edge of the panel were more curved than the lines near the center. Because one contour line was regarded to have the same β coordinate, the panel showed more distortion near the edge. The distortion can be reduced by carefully modifying Eqs. (2.12) and (2.13) to nonlinear equations.
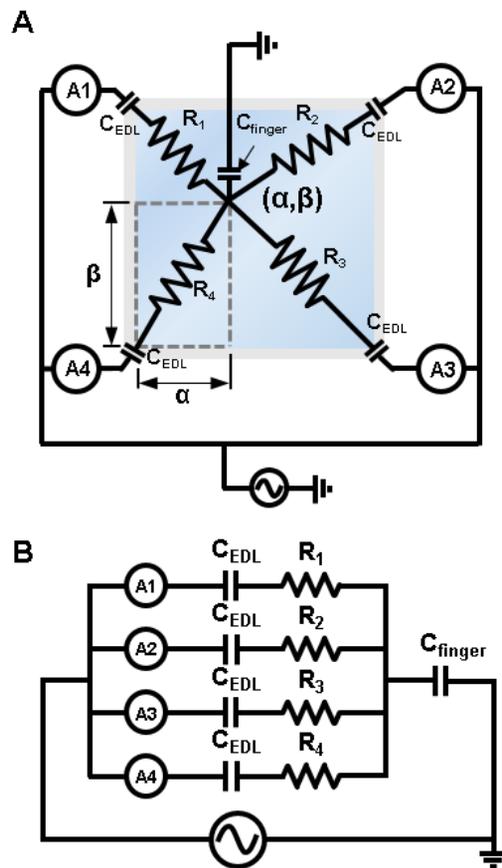
Fig. 2.10. (A) A schematic diagram of an ionic touch panel. A touched position was represented by two normalized distances, a and b. (B) An equivalent electrical circuit of the panel during touching.
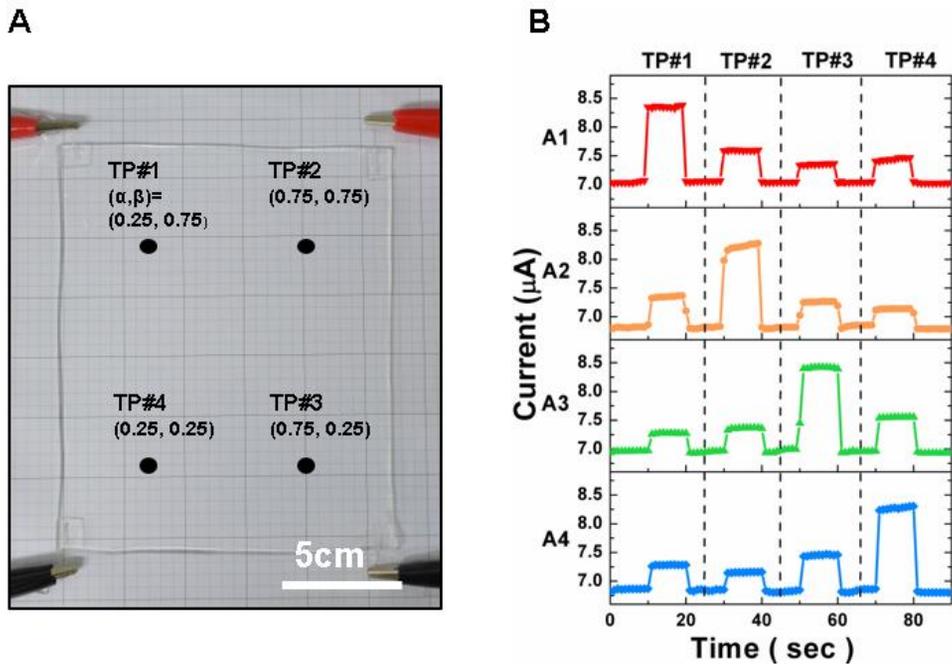
Fig. 2.11. (A) The panel was fully transparent and stable during operation. To reveal the sensitivity of position detection, four touch points (TP#1 to TP#4) of the panel were investigated. (B) FromTP#1 to TP#4, the points were sequentially touched, and the currents measured from the four current meters were plotted against time.
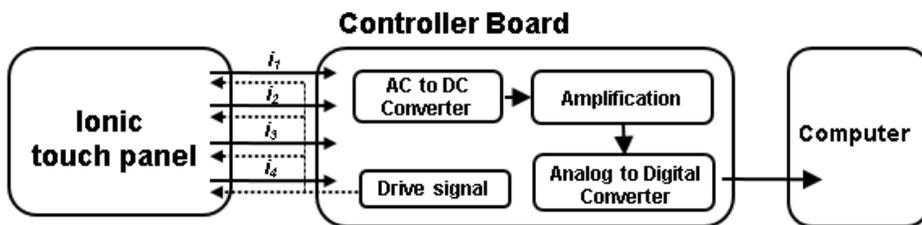
Fig. 2.12. A block diagram of a controller board that helps communication between the ionic touch panel and a computer.
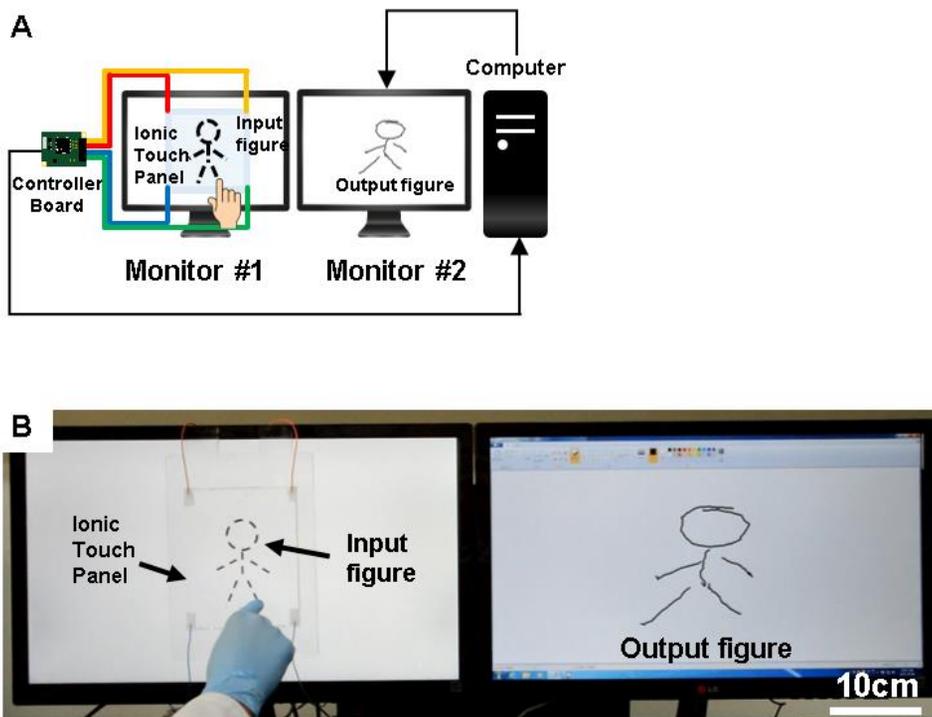
Fig. 2.13. Operation of the ionic touch panel was demonstrated with a dashed-man drawing. Monitor #1 displays the dashed man, and an ionic touch panel was attached to monitor #1. When a finger drew through the trace of the dashed man on the panel, the drawing was detected and transferred to a computer by the controller board. The output drawing was displayed on monitor #2.

A
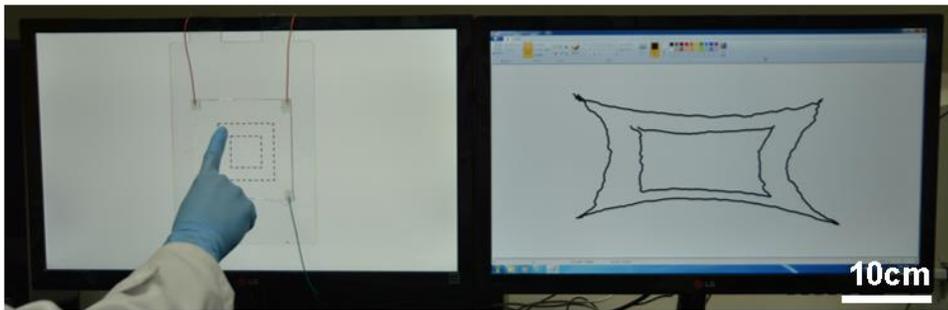
B
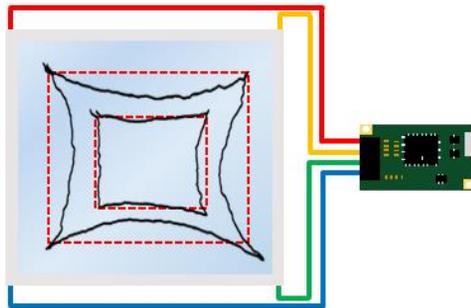
Fig. 2.14. The ionic touch panel showed distortion near the edges. Two concentric squares were tested on the panel, and the outer square showed more distortion than that of the inner square.
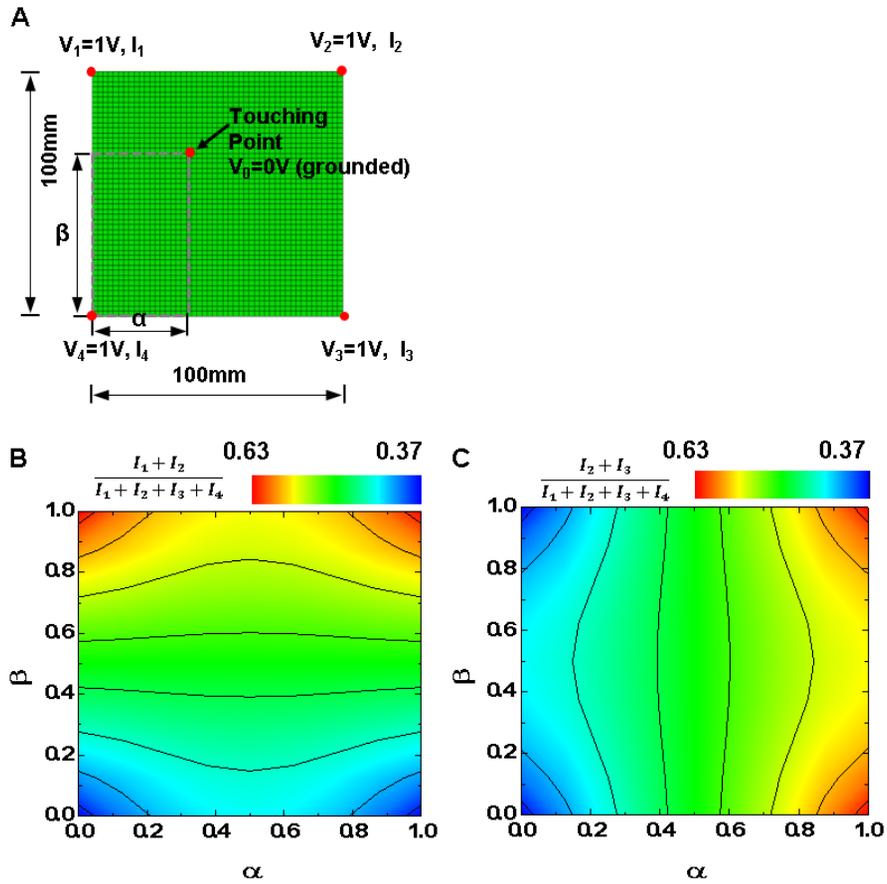
Fig. 2.15. A model for a FEM simulation. The same potential of 1 V was applied to the four corners of the panel, and the touch point at its position (α, β) was grounded as boundary conditions. (B and C) We calculated the current ratio from the simulation and plotted in (B) and (C), respectively. The nonlinearity of the resistance in a 2D panel caused the distortion.

2.3.9   A stretchable touch panel.

Experiments were performed to prove the stability of the touch panel in a stretched state. A circular touch panel with a diameter of 4 cm and a homemade biaxial stretcher (*24*) were prepared (Fig. 2.16A). The panel was glued to the biaxial stretcher and connected to the controller board via Pt electrodes. As shown in Fig. 2.16B, the diameter of the touch panel was enlarged after stretching up to 12.5 cm, which corresponded to 1000 % areal strain. As shown in Fig. 2.16C, the touch panel can even be operated under highly stretched states. The A1 currents of the touch panel at the undeformed and stretched states were measured with a touch point at the center in Fig. 2.17A. The baseline current increased from 6.68 µA to 9.16 µA according to the stretch of the panel. The increase in the baseline current is suspected to be related with an expansion of the surface area of the gel panel (Fig. 2.7.), and the baseline current shows insensitivity to strain rate in the range of 0.2–1/min (Fig. 2.8.). When the stretched panel was touched, current was added to the baseline currents. The touching currents in a stretched state were 0.52 µA and 0.45 µA at $\lambda =$ 2 and 3, respectively, which is similar to the current in the undeformed state (0.40 µA); the current response for a touch was not sacrificed by stretching. Fig. S4 shows the current changes caused by touch during the stretching of a gel strip. The baseline current gently increased, but the touching current was instantly increased when the strip was touched. Therefore, each current signal from stretching and touching can be distinguished by its slope as well. Four touch points were sequentially investigated with a square touch panel at a stretch of $\lambda = 1.5$ as shown in Fig. 2.17B. The negative correlation between distance and current was maintained in a stretched state. The panel could be operated with an anisotropic deformation. As shown in Fig. 2.20, the output figures were slightly shifted toward the undeformed edges after the

deformation. However, when we applied an additional position calibration after the deformation, the shift was compensated.

Electromechanical stability was tested for the hydrogel through a cyclic loading test up to 100 cycles (Fig. 2.18 and 2.19A). Fig. 2.19A presents the measured resistance at various cycles: 1, 5, 10, and 100 cycles. The resistance slightly increased as the cycles increased, showing a maximum variation of 25 % when $\lambda = 3$. We suspect that the increase in resistance during a cyclic test may originate from water evaporation in the gel. The weight of the gel decreased from 9.6 g to 7.54 g after the test. A uniaxial tensile test was performed with a hydrogel specimen as shown in Fig. 2.19B. The hydrogel showed an elastic modulus of 12 kPa and an elongation of $\lambda = 11$.
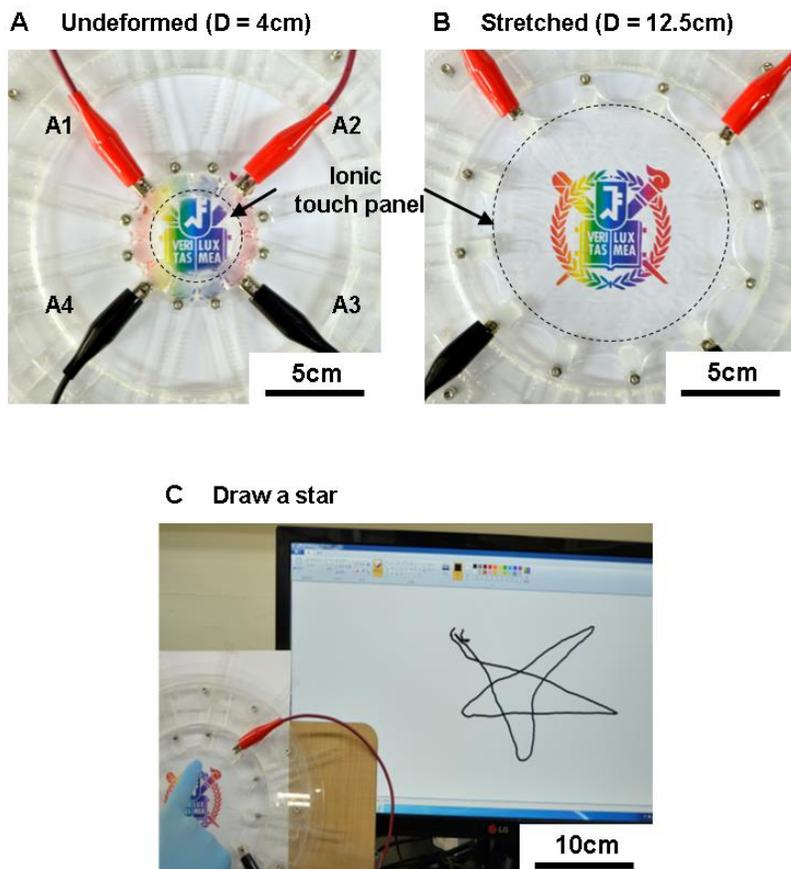
Fig. 2.16. (A and B) The ionic touch panel was stretched equibiaxially up to 1000% in area. A circular PAAm hydrogel film was glued to a biaxial stretcher, and the diameter of the hydrogel was increased from D = 4 cm to D = 12.5 cm. (C) The stretched touch panel was connected to a computer and operated as an input device.
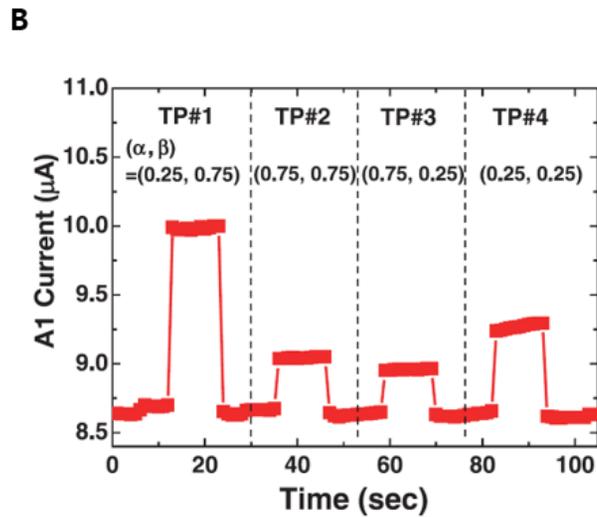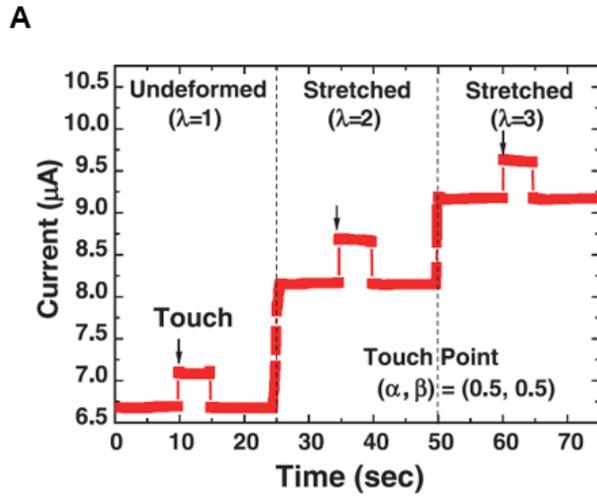
Fig. 2.17. (A) The A1 current was measured before ($\lambda = 1$) and after stretching ($\lambda = 2$ and $\lambda = 3$). The baseline current increased according to the stretch of the panel. However, the touching currents were insensitive to the stretching. (B) The A1 current was investigated for various touch points in a stretched state ($\lambda = 1.5$).
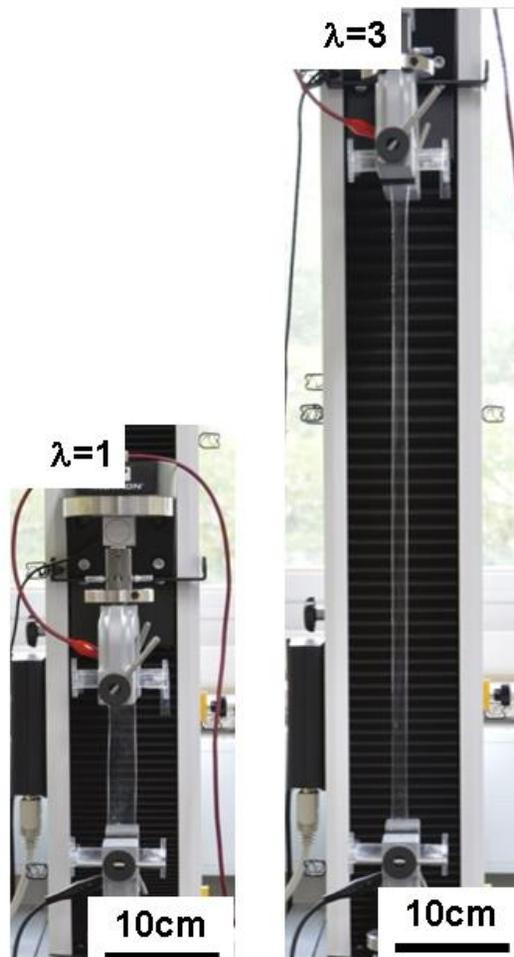
Fig. 2.18. An electromechanical test was performed on a hydrogel containing LiCl salts (2 M) up to 100 cycles.

A

B
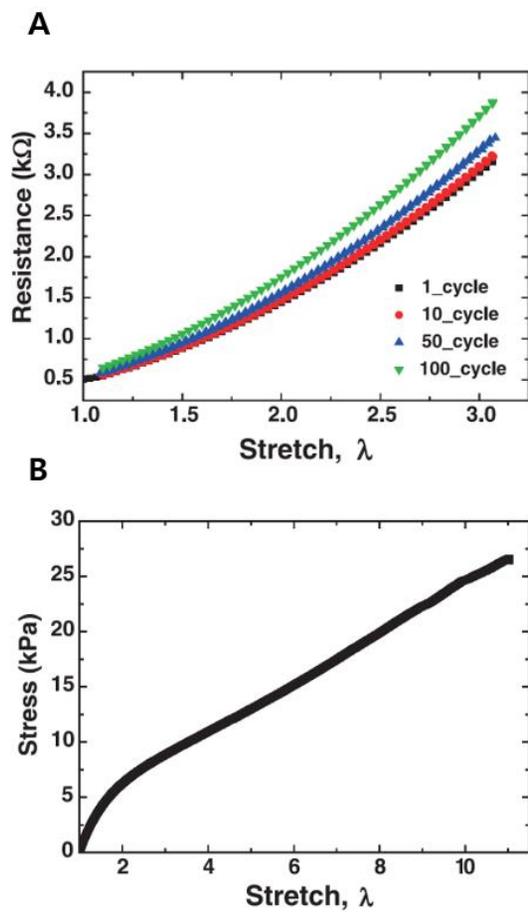
Fig. 2.19. (A) The resistance change of the gel strip was investigated during cyclic loadings. (B) A uniaxial tensile test was performed on a PAAm hydrogel.

2.3.10   Operation of an ionic touch panel under an anisotropic deformation.

We tested the operation of an ionic touch panel under an anisotropic deformation. As shown in Fig. 2.20, the panel was deformed into an anisotropic shape by pulling one corner or by stretching its edges to a trapezoid, and the panel was operated under an anisotropic deformation. We stretched the ionic touch panel by using a metal stretcher. The panel was insulated from the stretcher by applying a layer of VHB film. The localization of the deformation in the panel was determined by drawing two tetragons with the same center but different sizes. The output figures were slightly shifted toward undeformed edges after the deformation. However, when we apply an additional position calibration after the deformation, the shift was compensated. As shown in Fig. 2.20E and H, the panel can accurately capture the drawing signal near the center even under an anisotropic deformation. The distortion near the edges can be reduced by software support or design of the panel.
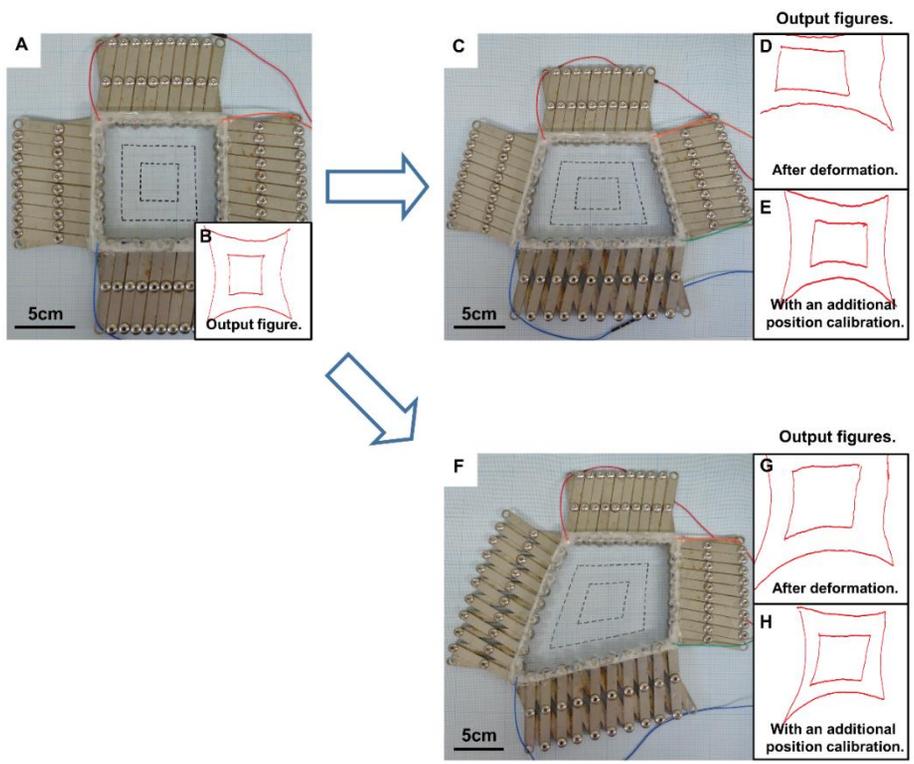
Fig. 2.20. Operation of an ionic touch panel under an anisotropic deformation. The ionic touch panel, which was a square of 10 cm on a side (A and B), was deformed into an anisotropic shape by stretching its edges to a trapezoid (C, D and E) or by pulling one corner (F, G and H). The output figures were slightly shifted toward undeformed edges after the deformation (D and G). However, when we applied an additional position calibration after the deformation, the shift was compensated (E and H).

2.3.11　An epidermal touch panel that is soft and transparent.

Fig. 2.21A shows a schematic design of an epidermal touch panel. The epidermal touch panel was built on a 1-mm thick VHB (3M) film to insulate the panel from the body. Because VHB film was originally developed as an adhesive, the panel could be attached to an arm without using extra glues (Fig. 2.21B). The epidermal touch panel was fully transparent such that it could convey visual content behind the touch panel. Moreover, the panel was mechanically soft and stretchable such that a user is comfortable with movement while wearing it. The currents measured before and after attachment are plotted in Fig. 2.22A. The baseline currents increased after the attachment owing to a leakage of charges through the VHB substrate. The thicker insulating layer generated a smaller baseline current. The effect of thickness of the insulating layers on the baseline currents is shown in Fig. 2.24. The sensitivity to touch decreased after the attachment; however, the touching current was still sufficient to be detected. As shown in Fig. 2.22B, we subsequently touched from TP#1 to TP#4 on the epidermal touch panel, and the current was measured with the A1 current meter. The correlation between the measured currents and the touched position was not influenced by the attachment. The epidermal touch panel could successfully perceive various motions, such as tapping, holding, dragging, and swiping. Thus, various applications can be easily managed by integrating the panel. As shown in Fig. 2.23, writing words (A), playing music (B), and playing chess (C) were accomplished via adequate motions on the epidermal touch panel.

A highly stretchable and transparent ionic touch panel was demonstrated. A polyacrylamide hydrogel containing 2 M LiCl salts was used as an ionic conductor. The mechanism of position sensing in an ionic touch panel was investigated with a

1-dimensional strip. The ionic touch strip showed precise and fast touch sensing even with a highly stretched state. We expand the position sensing mechanism to a 2-dimensional panel. We could draw a figure using the 2-D ionic touch panel. The ionic touch panel could be operated under more than 1000 % areal strain. An epidermal touch panel was developed based on the ionic touch panel. The epidermal touch panel could be applied onto arbitrarily curved human skin, and its use was demonstrated by writing words and playing the piano and games.

2.3.12   The insulation of the epidermal touch panel.

An experiment was conducted to determine the relation between the leakage current and the thickness of the insulating layer. When the epidermal touch panel is attached to the skin, an additional leakage current flows through the human skin. As a result, an increase in the leakage current provokes an increase in the baseline current and a decrease in the touching current, causing weakened sensitivity of the epidermal touch panel. The acrylic plate (1 mm thick) was used as a dielectric insulating layer. The thickness of the insulating layer was reduced from 6 mm to 1 mm in 1 mm decrements as shown in Fig. 2.24, and the baseline current decreased by 0.02 µA per 1 mm. Therefore, the touch sensitivity of the epidermal touch panel can be enhanced by applying sufficient insulation.
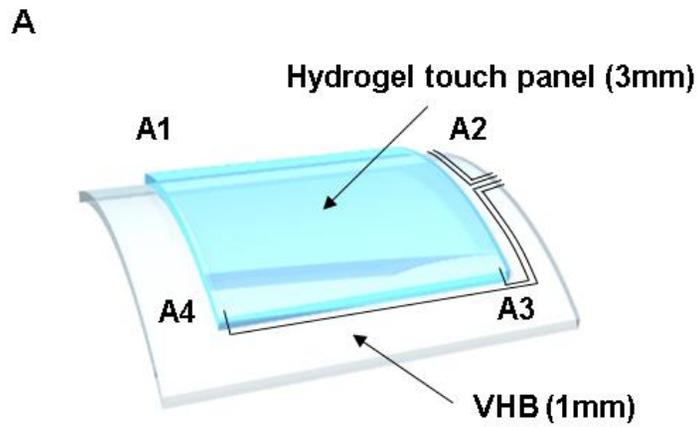
Fig. 2.21. (A) An epidermal touch panel was developed on a VHB substrate so as to insulate the panel from the skin and to mount the panel on a curved surface. (B) The touch panel was attached to an arm.
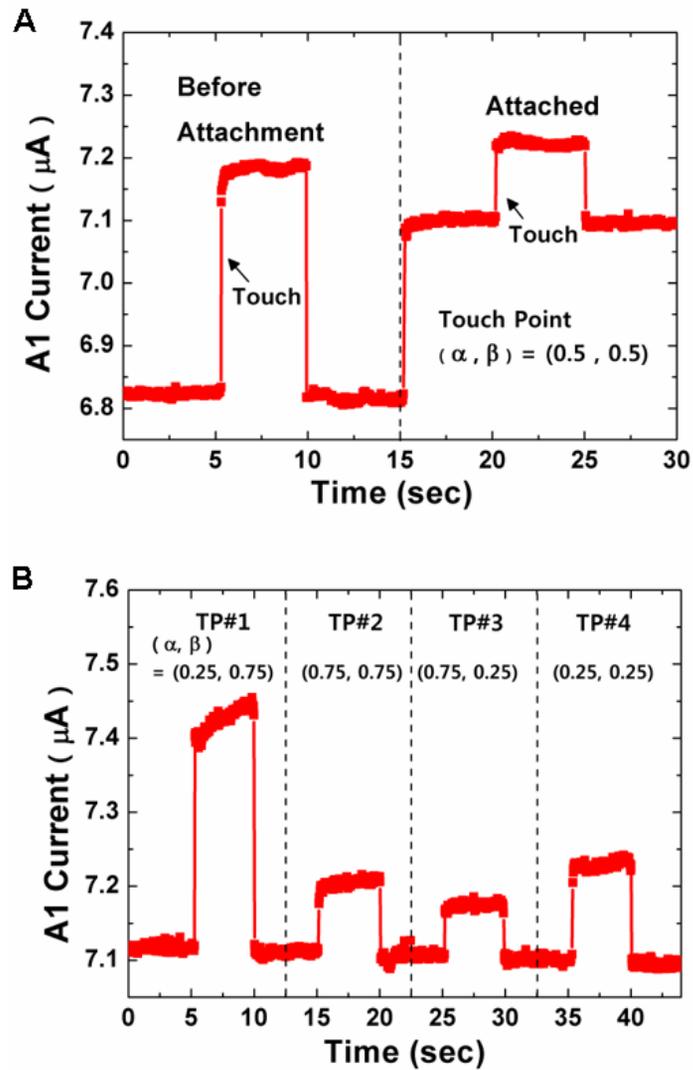
Fig. 2.22. (A) The A1 current of the panel was explored before and after attachment to an arm. (B) The position sensitivity after the attachment was tested by measuring the A1 currents at various touch points.
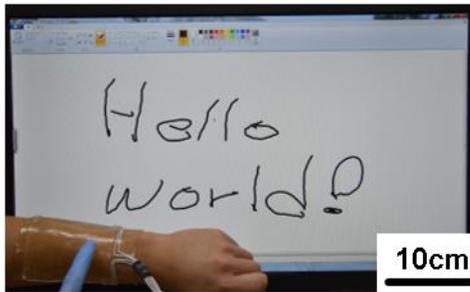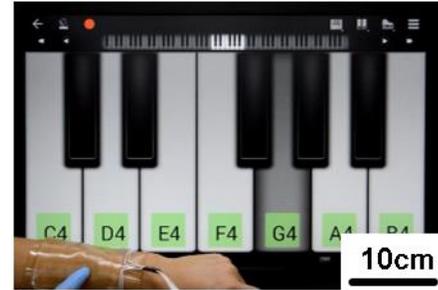
Fig. 2.23. The epidermal touch panel is capable of detecting motions, such as tapping, holding, dragging, and swiping. Demonstrations such as writing words (A), playing music (B), and playing chess (C) are shown.
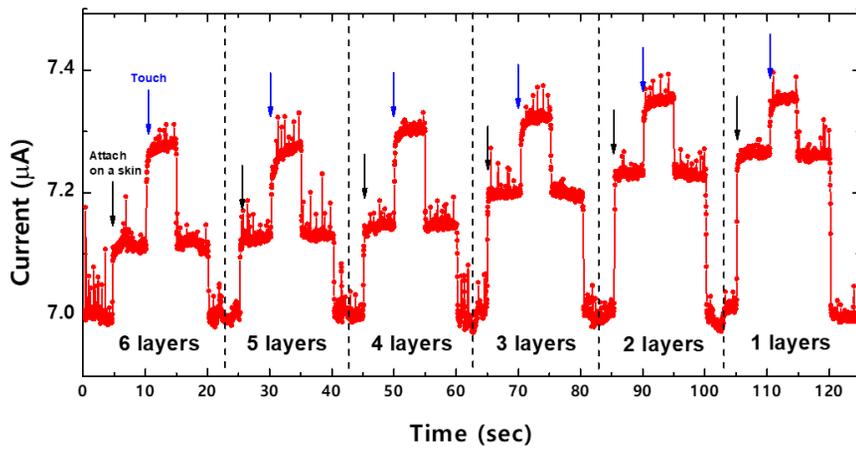
Fig. 2.24. The current is plotted against the number of insulating layers. The insulating layers were removed one by one. The thicker insulating layer allows the ionic touch panel to be more sensitive to touch signals.

2.4. Conclusion

An ionic touch panel containing LiCl salts was demonstrated for the first time. The ionic touch panel worked on a surface capacitive touch system in a typical working voltage range (- 0.6 V~ 0.6 V). The correlation between the distance and the current change was investigated in a 1-dimensional case and verified that it could operate even in a stretched state. In a 2-dimensional case, we could draw figures using the ionic touch panel. Because hydrogels are soft and stretchable, the hydrogel-based ionic touch panels could be stretched enormously (areal strain greater than 1000%) while retaining its transparency and functionality as a touch panel. Finally, the ionic touch panel could be integrated into arbitrarily curved human skin. We demonstrated writing words, playing the piano and games using the ionic touch panel attached to a human arm. Because flexible and stretchable devices are in demand at present and will be in future technologies, ionic touch panels made from hydrogels will be a good solution for stretchable and transparent input devices or sensors for applications that require a biological/ionic interface. Ionic devices based on hydrogels will lead the field of wearable, attachable sensing.

Reference

[1]   Thomas Young, Force sensitive touch panel. *U.S. Patent* 5,241,308 (1993).

[2]   R. Aguilar, G. Meijer, Fast interface electronics for a resistive touch-screen. *Proc. IEEE Sens.* **2**, 1360-1363 (2002)

[3]   S. P. Hotelling, J. A. Strickon, B. Q. Huppi, Multipoint touchscreen. *U.S. Patent* 7,663,607 (2010).

[4]   P. T. Krein, R. D. Meadows, The electroquasistatics of the capacitive touch panel. *IEEE Trans. Ind. Appl*. **26**, 529-534 (1990).

[5]   R. Adler, P. J. Desmares, An economical touch panel using SAW absorption. *IEEE Trans. Ultrason., Ferroelect., Freq.Control.* **34**, 195-201 (1987).

[6]   M. R. Bhalla, A. V. Bhalla, Comparative study of various touchscreen technologies. *Int. J. Comput. Appl.* **6**, 12-18 (2010).

[7]   Daniel Langley, Gael Giusti, Celine Mayousse, Caroline Celle, Daniel Bellet and Jean-Pierre Simonato, Flexible transparent conductive materials based on silver nanowire networks: a review. *Nanotechnology* **24**, 452001 (2013).

[8]   R. B. H. Tahar, T. Ban, Y. Ohya, Y. Takahashi, Tin doped indium oxide thin films: *Electrical properties. J. Appl. Phys.* **83**, 2631-2645 (1998).

[9]   M. Vosgueritchian, D. J. Lipomi, Z. Bao, Highly conductive and transparent PEDOT: PSS films with a fluorosurfactant for stretchable and flexible transparent electrodes. *Adv. Funct. Mater.* **22**, 421-428 (2012).

[10]   Y. Xia, K. Sun, J. Ouyang, Solution-processed metallic conducting polymer films as transparent electrode of optoelectronic devices. *Adv. Mater.* **24**, 2436-2440 (2012).

[11]   L. Hu, W. Yuan, P. Brochu, G. Gruner, Q. Pei, Highly stretchable, conductive, and transparent nanotube thin films. *Appl. Phys. Lett.* **94**, 161108 (2009).

[12] Zhuangchun Wu, Zhihong Chen, Xu Du, Jonathan M. Logan, Jennifer Sippel, Maria Nikolou, Katalin Kamaras, John R. Reynolds, David B. Tanner, Arthur F. Hebard, Andrew G. Rinzler, Transparent, conductive carbon nanotube films. *Science* **305**, 1273-1276 (2004).

[13] Zang, J., Ryu, S., Pugno, N., Wang, Q., Tu, Q., Buehler, M. J., & Zhao, X. (2013). Multifunctionality and control of the crumpling and unfolding of large-area graphene. *Nat. Mater*. **12**, 321-325 (2013)

[14] Zang, J., Ryu, S., Pugno, N., Wang, Q., Tu, Q. *et al.* Roll-to-roll production of 30-inch graphene films for transparent electrodes. *Nat. Nanotechnol.* **5**, 574-578 (2010).

[15] L. Hu, H. S. Kim, J.-Y. Lee, P. Peumans, Y. Cui, Scalable coating and properties of transparent, flexible, silver nanowire electrodes. *ACS nano* **4**, 2955-2963 (2010).

[16] S. De, T. M. Higgins, P. E. Lyons, E. M. Doherty, P. N. Nirmalraj, W. J. Blau, J. J. Boland, J. N. Coleman, Silver nanowire networks as flexible, transparent, conducting films: extremely high DC to optical conductivity ratios. *ACS nano* **3**, 1767-1774 (2009).

[17] Guo, C. F., Liu, Q., Wang, G., Wang, Y., Shi, Z. *et al*., Fatigue-free, superstretchable, transparent, and biocompatible metal electrodes. *Proc. Natl. Acad. Sci. U.S.A.* **112**, 12332-12337 (2015).

[18] O. Akhavan, E. Ghaderi, Toxicity of graphene and graphene oxide nanowalls against bacteria. *ACS nano* **4**, 5731-5736 (2010).

[19] L. Ding et al., Molecular characterization of the cytotoxic mechanism of multiwall carbon nanotubes and nano-onions on human skin fibroblast. *Nano Lett.* **5**, 2448-2464 (2005).

[20] Sun, J. Y., Zhao, X., Illeperuma, W. R., Chaudhuri, O., Oh, K. H. *et al.*, Highly stretchable and tough hydrogels. Nature 489, 133-136 (2012).

[21] Y. Qiu, K. Park, Environment-sensitive hydrogels for drug delivery. *Adv. Drug Deliv. Rev.* **64**, 49-60 (2012).

[22] Darnell, M. C., Sun, J. Y., Mehta, M., Johnson, C., Arany, P. R., Suo, Z., & Mooney, D. J., Performance and biocompatibility of extremely tough alginate/poly-acrylamide hydrogels. *Biomaterials* **34**, 8042-8048 (2013).

[23] Obara, K., Ishihara, M., Ishizuka, T., Fujita, M. *et al.*, Photocrosslinkable chitosan hydrogel containing fibroblast growth factor-2 stimulates wound healing in healing-impaired db/db mice. *Biomaterials* **24**, 3437-3444 (2003).

[24] Keplinger, C., Sun, J. Y., Foo, C. C., Rothemund, P., Whitesides, G. M., Suo, Z., Stretchable, transparent, ionic conductors. *Science* **341**, 984-987 (2013)

[25] J. Y. Sun, C. Keplinger, G. M. Whitesides, Z. Suo, Ionic skin. *Adv. Mater* **26**, 7608-7614 (2014).

[26] Larson, C., Peele, B., Li, S., Robinson, S., Totaro, M. *et al.*, Highly stretchable electroluminescent skin for optical signaling and tactile sensing. *Science* **351**, 1071-1074 (2016).

[27] W. Pepper Jr. Touch panel system and method *U.S. Patent*. 4,293,734 (1981).

[28] Gong, L. X., Wang, R. Z., Xia, Z. Z., & Chen, C. J.. Adsorption equilibrium of water on a composite adsorbent employing lithium chloride in silica gel. *J. Chem. Eng. Data*. **55,** 2920-2923 (2010).

[29] Hudson, John L, T. T. Tsotsis. Electrochemical reaction dynamics: a review. *Chem. Eng. Sci.* **49**, 1493-1572 (1994).

[30] Haga, H., Yanase, J., Kamon, Y., Takatori, K., Asada, H., Kaneko, S., 45.1: Touch Panel Embedded IPS-LCD with Parasitic Current Reduction Technique, *SID Symp. Dig.Tec.* **41**, 669-672 (2010)

[31] H. Tian et al., A novel flexible capacitive touch pad based on graphene oxide film, Nanoscale 5, 890-894 (2013).

Chapter 3. Ionic wireless power transfer

3.1. Introduction

Advances in implantable biomedical devices have led to improvement in areas such as long-term monitoring, diagnostic, and treatment [1]. As the devices become more complex and the amount of information delivered increases, the power consumption of the devices is also increased [2]. So it has been one of the major challenges to supply enough power to the implantable device. The typical power source used in implantable devices is the battery [3]. But it is not suitable for the long term therapy because the battery takes a lot of space in a body and requires invasive surgery for the replacement [4, 5]. Another alternative is harvesting energy from the implant's surroundings [6-8]. However, the amount of available energy is often insufficient for medical systems. Therefore, Wireless power transfer (WPT) systems have been developed in that a continuous supply of energy is provided in sufficient quantities.

While several WPT systems have been proposed for biomedical implants, inductive power transfer (IPT) [9, 10] system is the most common and well-established method of power transfer. The IPT systems deliver the power using two coils coupled via magnetic field. The transmitting coil generates time-varying magnetic field and induce current in the receiving coil. Since the efficiency of the IPT depends on the resistance of the coil, which are made of metal with high electrical conductivity. However, stiffness of metal is not compatible with the surrounding tissues, so the coils are fabricated in the form of serpentine pattern or metal nanowires embedded in polymers to increase the flexibility and stretchability

[11-14]. Capacitive power transfer (CPT) has been proposed as an alternative to IPT, exhibiting simple structure, design flexibility, excellent misalignment performance, low cost, and low weight [15, 16]. The CPT systems deliver the power by using an electrostatic induction between two capacitively coupled plates. Since the capacitive coupling can be achieved even with materials that are less conductive than metals, the use of CPT systems can expand the choice of the materials. However, CPT systems with non-metallic couplers have not been explored yet, and the most CPT systems are delivering power through metal plates. The metallic couplers in CPT systems still have problems such as biocompatibility and mechanical mismatches, making them difficult to apply to biomedical implants.

Ionic conductors have recently attracted attention as an alternative for conventional conductive materials. In the ionic conductor, the current is transported by mobile ions in the electrolyte solution [17]. Since liquid electrolytes are easy to leak even when encapsulated, solid-like electrolytes capable of stable encapsulation have been introduced and broaden the range of applications [18, 19]. Hydrogel, a representative solid-like electrolyte, is stretchable and biocompatible while exhibiting comparable ionic conductivity to the liquid electrolyte. Several types of ionic devices employing hydrogels have been developed, including actuator [20, 21], strain sensor [22], touch sensor [23, 24], electroluminescent skin [25], and energy generator [26]. In the ion devices, electrochemical reactions can be generated at the interface between ionic conductor and electrode. Since the electrochemical reactions in the ionic devices are typically considered to cause side effects such as electrode dissolution and gas generation, the ionic devices prevent the electrochemical reactions by lowering the applied voltages at the interface. However, electrochemical reactions can be a unique feature of the ionic system, and if it can be controlled, the

ionic devices can derive a variety of functions that are not available in traditional electronics.

We demonstrate herein the ionic wireless power transfer (IWPT) system operated on the basis of ionic currents. In our IWPT system, power is transferred wirelessly via capacitively coupled pair; An ion conductive hydrogel plate act as a receiver and a metal plate act as a transmitter. The operations of the IWPT were explored under various conditions. Power was even delivered to the subcutaneous site of the mouse via IWPT system. Furthermore, the charge accumulation caused by the prevention of discharge on the electrical double layer (CAPDE) enables the IWPT to electrochemically synthesize products during the power transfer. The mechanism of the CAPDE was studied and NADPH, reducing agent in anabolism, was synthesized by the CAPDE system.

3.2. Experimental section and backgrounds

3.2.1   Materials and synthesis

Gel receivers were made with PAAm hydrogel and NaCl salt. Acrylamide (AAm; A8887; Sigma) and N,N-methylenebisacrylamide (MBAA; M7279; Sigma) were used as the monomer and cross-linking agent for the PAAm gel, respectively. Ammonium persulfate (AP; A9164; Sigma) and N,N,N',N'-tetramethylethylenediamine (TEMED; T7024; Sigma) were used as the thermal initiator and accelerator for gelation, respectively. NaCl (S7653; Sigma) was used as the ionic charge carrier. PDMS (Silgard 184) was used for encapsulation of the IWPT device. Copper was used as the transmitter and for interconnecting wires in the IWPT device. 1N5711 Schottky diodes were used in the rectifier circuit. Nicotinamide adenine dinucleotide phosphate (NADP$^+$; NADP-RO; Sigma), and PBS buffer (P5493; Sigma) were used to synthesize the gel receiver used for NADPH reduction. The Ti foil (0.127-mm-thick; Alfa Aesar), SS foil (0.1-mm- thick; Alfa Aesar), Pt foil (0.1-mm-thick; Alfa Aesar) and silver foil (Ag, 1-mm-thick; Alfa Aesar) were cut into 2×0.5 cm^2 sections, polished with sandpaper, sonicated in acetone, ethanol and distilled water, and dried in an oven at 50°C before use. An Ag/AgCl CE was prepared electrochemically by passing 10 mA/cm^2 through an Ag electrode for 10 min in 0.1 M HCl.

Ionic hydrogels were synthesized using a solution-based method. A monomer solution of AAm (2.17 M) was prepared and MBAA (0.06 wt%) and aminopropyltriethoxysilane (APS; 0.16 wt%) were added as the cross-linking agent and initiator, respectively. The amount of salt was adjusted according to the experiment. After degassing via ultrasonication, TEMED (0.25 wt%) was added to

the monomer solution as an accelerator. After careful mixing, the monomer solution was poured into a polymethylmethacrylate (PMMA) mold and covered with a PMMA plate to prevent contact with air. The solutions were polymerized at room temperature for 2 hours. For gel receivers to be used for NADPH generation, PBS buffer solutions containing 1 mM $NADP^+$ were used instead of deionized water.

3.2.2   Experimental setup for IWPT

The IWPT receiver was made of poly acrylamide hydrogel containing 1 M NaCl. Any metallic components, particularly the electrodes, on the receiving side may affect transmission efficiency. Therefore, the receiver was shaped such that metallic components and the transmitter were as far apart as possible. The gel receiver was fabricated as a long rectangle (width: 20 mm; length: 120 mm; thickness: 2 mm) and electronic parts on the receiving side were placed at the end of the receiver farthest from the transmitter. The length and width of the gel receiver were determined by considering the resistance of the current path through which the transmitted current flows. The transferred current was measured using current meters (model 34461A; Agilent). Since the current meters were not able to measure at frequencies of 10 MHz, the delivered current was rectified through 1N5711 Schottky diodes and measured in DC mode. Schottky diodes feature low forward voltage drop and a very high switching rate, resulting in low distortion at high input frequencies.

3.2.3   Power transfer in series resistor–inductor–capacitor (RLC) circuits.

IWPT systems rely on LC resonance to overcome the high impedance that results from the small capacitance of the coupling capacitor. An IWPT system can be represented by a circuit in which a resistor, inductor, and capacitor are connected

in series as an RLC circuit (Fig. 3.1A). In a series RLC circuit, the currents flowing, R, L, and C, are equal and in phase at all times. However, the voltage across L leads the current by 90° and the voltage across C follows the current by 90°. Since the phase difference between the voltages across L and C is 180°, they cancel each other out (Fig. 3.1B). The total impedance in the series RLC circuit can be represented by the following equations:

$$Z_{total} = R + Z_L + Z_C$$

$$= R + jX_L + jX_C$$

$$= R + j\left(\omega L - \frac{1}{\omega C}\right) \tag{3.1}$$

where R is the resistance, Z_L and Z_C are the impedances of L and C, X_L and X_C are the reactances of L and C, j is an imaginary unit, and ω is the angular frequency. When the angular frequency reaches a certain value, the reactances of L and C become equal in magnitude and opposite in sign. Total impedance then consists solely of pure resistance with a minimal value, resulting in maximum current flow through the circuit. This point is called resonance and the frequency at which this occurs is called the resonance frequency. The current flowing the circuit at the resonance frequency is determined by

$$i = \frac{V_S}{Z_{total}} = \frac{V_S}{R} \tag{3.2}$$

and the voltage across each component in the RLC circuit can be represented by the following equations:

$$V_R = iR = V_S \tag{3.3}$$

$$V_L = iX_L = V_S \frac{X_L}{R} \tag{3.4}$$

$$V_C = iX_C = V_S \frac{X_C}{R} \tag{3.5}$$

where V_S, V_R, V_L, and V_C are the voltages across the source, R, L, and C, respectively. At the resonance frequency, the voltage applied to R is the same as the source voltage. In our IWPT system, however, the reactance of the components is larger than R, so that the voltages across L and C are larger than the source voltage. Using an amplified voltage across the coupling capacitor allows the current to be transferred through a small coupling capacitor. However, small capacitors require larger voltages across C, which causes voltage stress. System parameters must therefore be optimized to minimize the effects of voltage stress on system efficiency.

A

L : 50μH   C : 5pF   R : 1kΩ

Inductor   Capacitor   Resistor

Signal generator
: -1V~1V

B

V_L : leads the current

V_C : lags the current

V_R : in-phase with the current

Voltage (V)

Time (ns)
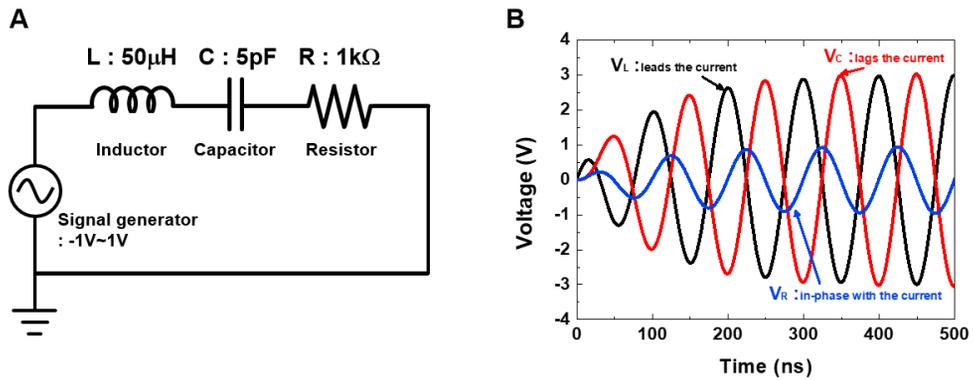
Fig. 3.1. A series resistor–inductor–capacitor (RLC) circuit can be used to represent the IWPT system and provide simulated voltages at each component. At the resonance frequency, voltages across the inductor and capacitor are completely canceled and the voltages at the signal generator and across the resistor are identical.

3.2.4   The structure of the coupling capacitor.

    IWPT operates based on CPT systems. CPTs can exhibit several types of coupler structure, depending on the number and arrangement of the coupling plates. Unipolar and bipolar systems are the most common capacitive coupler structures, with the unipolar configuration having the simplest structure (Fig. 3.2A). Unipolar systems are also called two-plate systems because they consist of two plates. One plate is used as a transmitter and the other as a receiver; each plate is connected to ground. The two plates form a single capacitor through which power is transferred. However, unipolar systems are limited in cases where it is difficult to ground to the receiver, such as inside the human body.

    Bipolar structures consist of four plates (Fig. 3.2B). Two transmitters and two receivers form two capacitors. One capacitor is connected to the signal generator and receives the input power. The other capacitor is connected to ground and provides the return path for the current. The receiver unit is connected to both the signal generator and ground via a coupling capacitor and receives power completely wirelessly. In this study, both systems were used according to their characteristics. The data shown in chapter 3.3.2 and 3.3.3 were collected using a unipolar system. This is because the receiver is connected to ground during current measurements. Bipolar configurations were used to show that IWPT systems can deliver power wirelessly. The demonstration system shown in chapter 3.3.1, the implantable device in chapter 3.3.3, and the IWPT system used for electrochemical reactions in chapter 3.3.4 were constructed with bipolar systems.
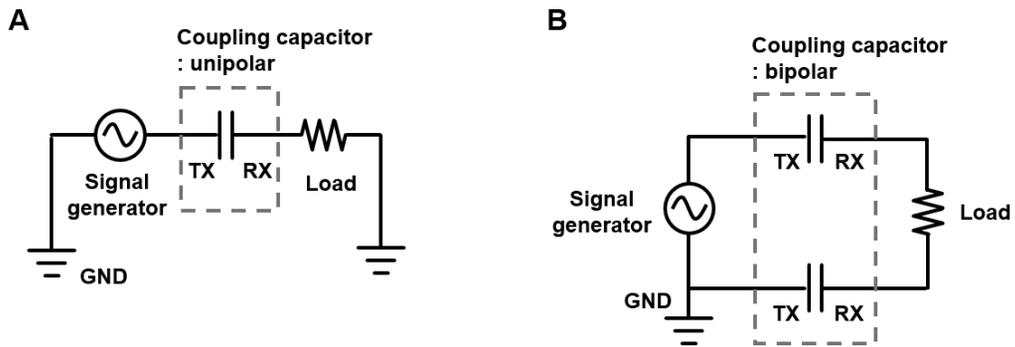
Fig. 3.2. System classification according to the structure of the coupling capacitor.

3.3. Results and Discussion

3.3.1   Basic principles and operations of an Ionic wireless power transfer (IWPT)

A schematic of an IWPT system is shown in Fig. 3.3. Electric power is transferred between two separate conductive plates. The transmitter is made of metal, while the receiver is composed of a hydrogel filled with a sodium chloride (NaCl) solution (1 M). An alternating current (AC) voltage source and an inductor for compensation are connected to the metal transmitter. A rectifier and a load are connected to the hydrogel receiver. The two plates (Tx and Rx) are arranged parallel to each other and act as a capacitor that allows AC to pass. The working principle of an IWPT is illustrated in Fig.3.4. When a voltage is applied across the transmitter and the receiver, charges in the transmitter attract ions in the receiver having the opposite charge, and repel ions having the same charge. If the voltage rapidly changes polarity, *i.e.*, an AC voltage is applied, then the coupling capacitor alternately charges and discharges, causing current to flow in the receiver. However, since the area available for coupling is limited, the capacitance of the Tx/Rx pair is only a few tens of picofarads, corresponding to very little charge storage or current transfer. Thus, we inserted an inductor between the power source and the coupling capacitor to construct an LC resonant circuit, as described in chapter 3.2.3. The LC resonance circuit amplifies the voltage between the transmitter and receiver, allowing more current to be transferred to the receiver. The resonance frequency (f_0) is determined by the inductance (L) and capacitance (C) of the system, and can be calculated using the following equation.

$$f_0 = \frac{1}{2\pi}\sqrt{\frac{1}{LC}} \tag{3.6}$$

Fig. 3.5 shows an IWPT system in use. The metal transmitter and gel receiver were separated by a 2-mm insulator. When an AC signal was applied to the metal transmitter, the green light-emitting diode (LED) connected to the receiving side lit up without any direct contact with the transmitter. The LED remained powered even when lifted 5 cm in the air. A rechargeable Li-ion battery was then connected as a load in the IWPT system to evaluate the performance of the IWPT system as a battery charger. The insulating layer was 2mm and the resonance frequency was 4.4 Mhz. The resulting charging curve is shown as a blue line in Fig. 3.6. The theoretical capacity of the battery is 13.6 mAh and the measured current at the receiving side was about 1.4 mA. For comparison, the battery was charged with wire-based charging system. Direct current (DC) source (Model B2901; Agilent) supplied a constant current of 1.4 mA to charge the battery (yellow line). The two curves show that the charges corresponding to the measured current was stored to the battery by the IWPT.
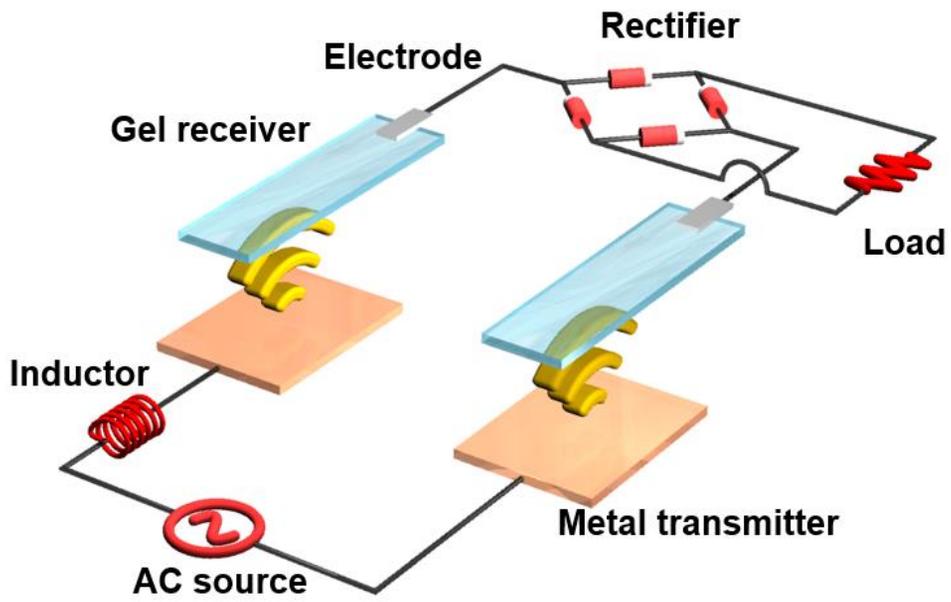
Fig. 3.3. Schematic of an IWPT system. A metal transmitter and a gel receiver comprise a coupled capacitor. An input signal, generated from an AC source, is transmitted to the gel receiver through an electrical field.
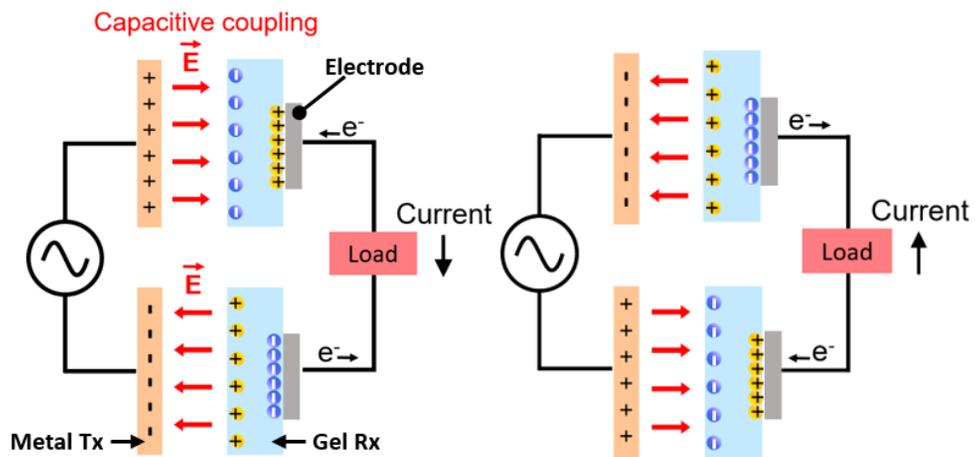
Fig. 3.4. The working principle of IWPT. Voltage applied to the transmitter induces polarization and movement of ions in the gel receiver, *i.e.*, an electrical current.
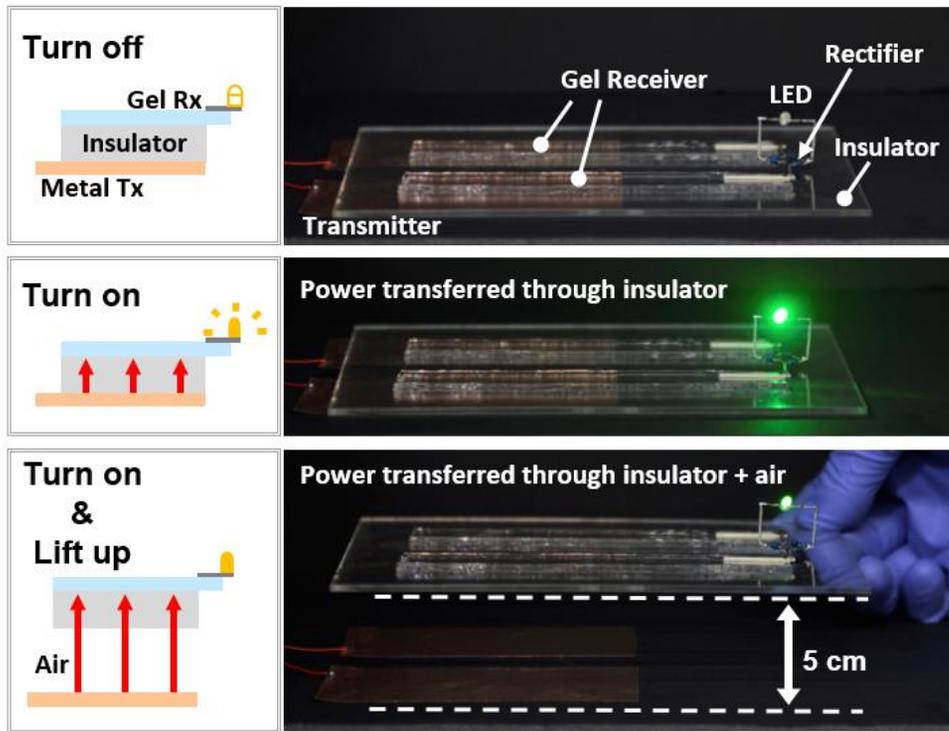
Fig. 3.5. Operation of an IWPT system. Electrical power was transferred from a copper layer to a gel layer through a 2-mm electrical insulator, and even through several centimeters of air.
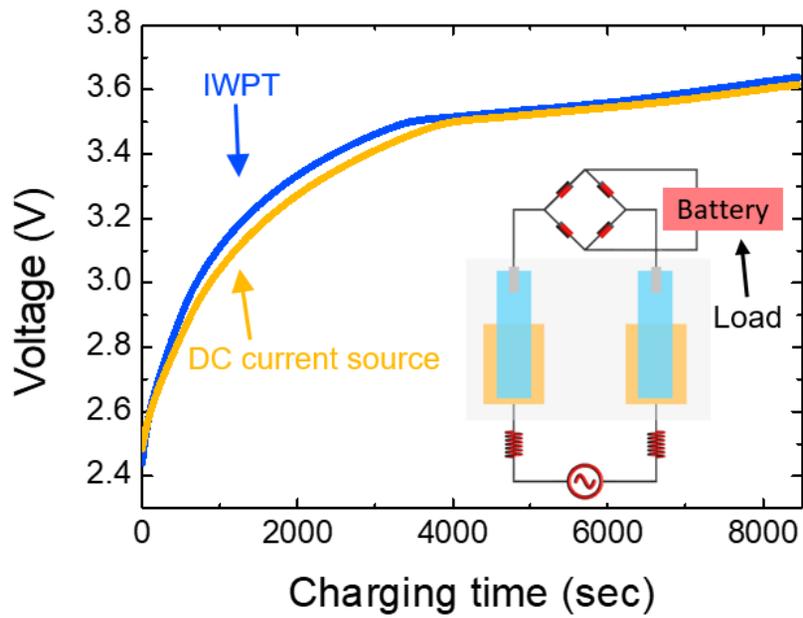
Fig. 3.6. Charging curves of the Li-ion batteries. IWPT systems can be used to charge Li-ion batteries. The battery was charged with 1.4 mA transferred across a 2-mm insulating layer.

3.3.2 Characteristics of IWPT

The ability of the IWPT system to transfer power was evaluated as a function of ion concentration, thickness, and the area of the hydrogel receiver. The transmitted AC was converted to DC through a rectifier circuit (Schottky diode; 1N5711) and measured with a current meter (model 34461A; Agilent). Experiments were conducted in a unipolar configuration, as described in chapter 3.2.4. The metal transmitter was made of copper tape (width: 50 mm; length: 70 mm) and the receiver was made of a PAAm hydrogel containing 1 M NaCl solution (width: 20 mm; length: 120 mm; thickness: 2 mm). The metal transmitters and gel receivers were separated by a 5-mm insulator. A 50-μH inductor was used for compensation of the coupling capacitor. A 1-kOhm resistor was connected to the receiver as a load. Fig. 3.7A shows the measured current as a function of transmission frequency with various ion concentrations in the gel receiver. The amplitude of the input voltage is 10 V and the frequency was swept from 1 Hz to 10 MHz. A maximum current of approximately 3.5 mA was obtained at the resonance frequency with a gel containing 4 M NaCl. The coupling capacitance and resonance frequency as a function of ion concentration are presented in Fig. 3.7B. The coupling capacitance between the metal transmitter and the gel receiver at 1 MHz was measured using an LCR meter (model E4980A; Agilent). The coupling capacitance remained constant at ~15 picofarads except at low ion concentrations in the gel (< 0.05 M). Resonance frequencies were consistent with values calculated by using Eq. (3.6). Capacitance refers to the ratio of the amount of charge stored in a capacitor to the potential difference across its plates. Applying 1 V to the coupling capacitor yielded a charge of 15 picocoulombs, which is equivalent to $\sim 10^{-16}$ moles. Thus, the amount of ions required to charge the

coupling capacitor is extremely low compared to the amount of ions contained in the receiver. Therefore, coupling capacitance was independent of ion concentration in the gel receiver.

However, as shown in Fig. 3.7C, the IWPT system transferred higher current when the ion concentration in the gel receiver was high. This effect can be explained by a decrease in the resistance of the gel receiver. The series resistance of the coupling capacitor is also presented in Fig. 3.7C. At the resonant frequency, because the impedance of the capacitor is compensated by the inductor, current is determined by the load and the series resistance of the capacitor. The electrode materials, internal wiring, and contacts in the coupling capacitor result in series resistance and power loss. The resistance of the gel receiver also affects the series resistance. The presented results indicate that high ion concentrations can lower the resistance of the gel receiver and enhance the current delivered through the IWPT system.

The influence of gel receiver thickness on the power transfer efficiency of our IWPT system is shown in Fig. 3.8A. Instead of a hydrogel, these experiments were performed using a NaCl solution in a receiver mold. The thickness of the receiver was varied between 1 and 12 mm by adding NaCl solution to the mold. Higher currents were delivered to thicker receivers, while maximum currents were measured at a constant frequency regardless of thickness. The resulting capacitance and resonance frequencies are presented in Fig. 3.8B. In all cases, these values remained constant, demonstrating that the amount of electric charge stored in the capacitor was not affected by the thickness of the hydrogel. In contrast, the amount of transferred current increased gradually with the thickness of the receiver and approached a plateau at thicknesses above 6 mm (Fig. 3.8C). This is because the

resistance of the receiver depends on the thickness of the receiver, which is proportional to the cross-sectional area of the current path. Therefore, thicker receivers allow more current to be delivered to the receiving side.

The effects of changing the capacitive area of the gel receiver were also evaluated, by varying the width of the gel receiver while maintaining the width of the transmitter at 50 mm and the overlapping length of the transmitter and receiver at 60 mm. Fig. 3.9A shows that the maximum current and resonance frequency changed simultaneously with changes in coupling area. Capacitance is proportional to the area of the capacitor and changes in capacitor area will change the resonance frequency. Thus, changing the width of the gel receiver from 5 to 50 mm resulted in a decrease in the resonance frequency from 6.0 to 4.2 MHz (Fig. 3.9B). The observed changes in maximum current can be accounted for by increases in the cross-sectional area of the gel receiver. Increasing the cross-sectional area of the gel receiver decreases its series resistance and allows more current to flow through the receiving side of the IWPT (Fig. 3.9C).
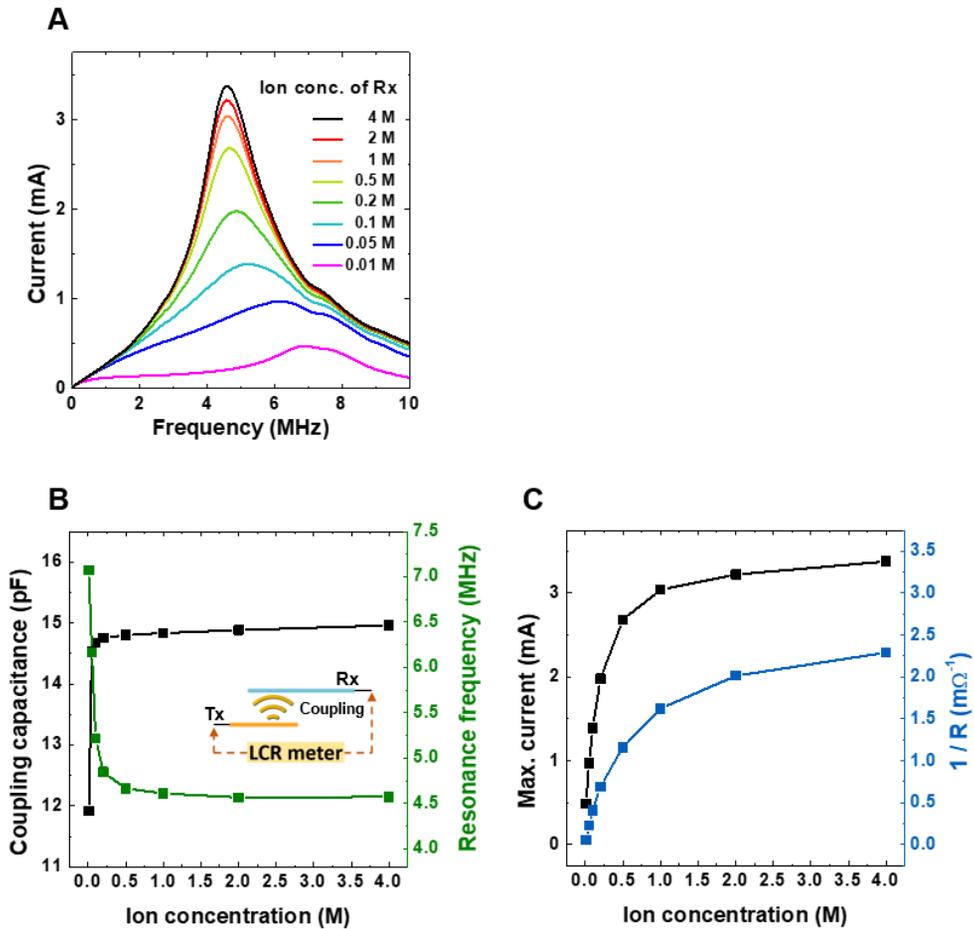
Fig. 3.7. (A) Electrical current was measured at the receiver as a function of transmission frequency and ion concentration in the gel receiver. (B) Coupling capacitance was measured between the transmitter and the receiver at 1 MHz. Coupling capacitance was insensitive to changes in ion concentration except at low ion concentrations (< 0.05 M). The resonance frequency was also constant as a function of ion concentration. (C) Maximum currents and the reciprocals of series resistance of the coupling capacitor are shown as a function of ion concentration. The resistance of the gel receiver results in ohmic losses in the IWPT, which in turn hinders the transfer of current to the receiver.
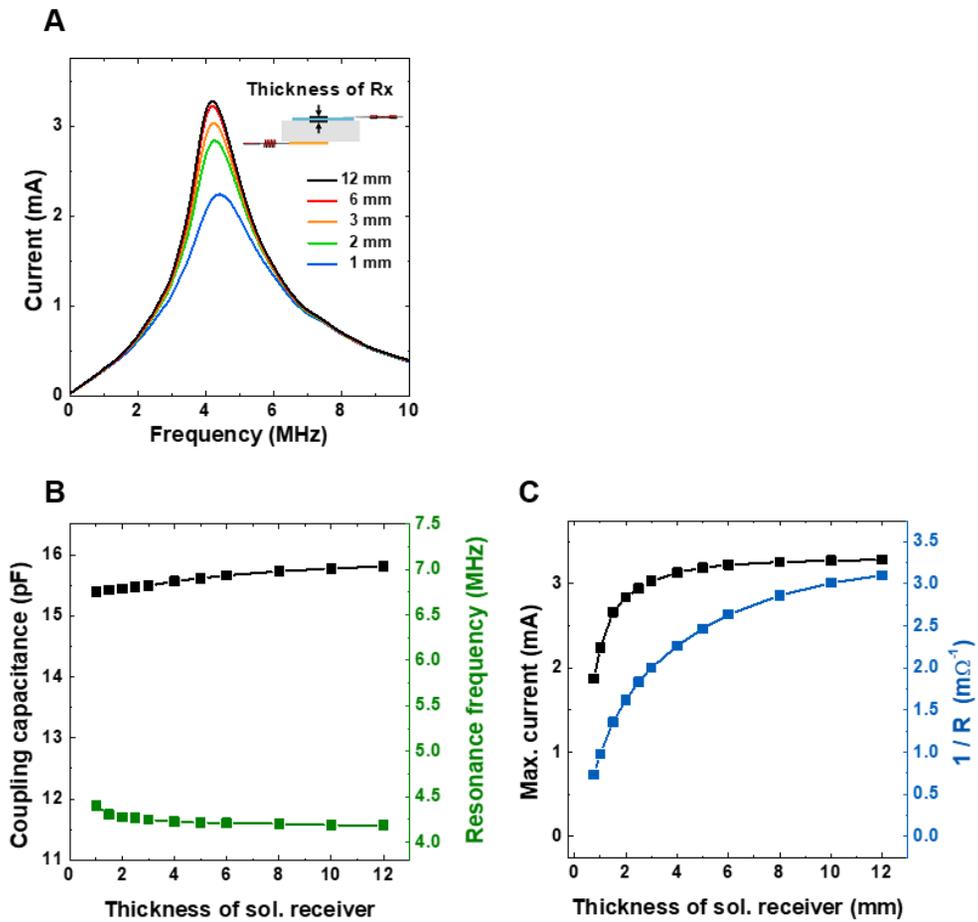
Fig. 3.8. (A) Current measured at the receiver is shown as a function of frequency and the thickness of the receiver. (B) Coupling capacitance and resonance frequency were constant regardless of the thickness of the gel receiver. (C) The thick receiving gel has a low resistance due to its larger cross-sectional area, which results in higher currents at the receiver.
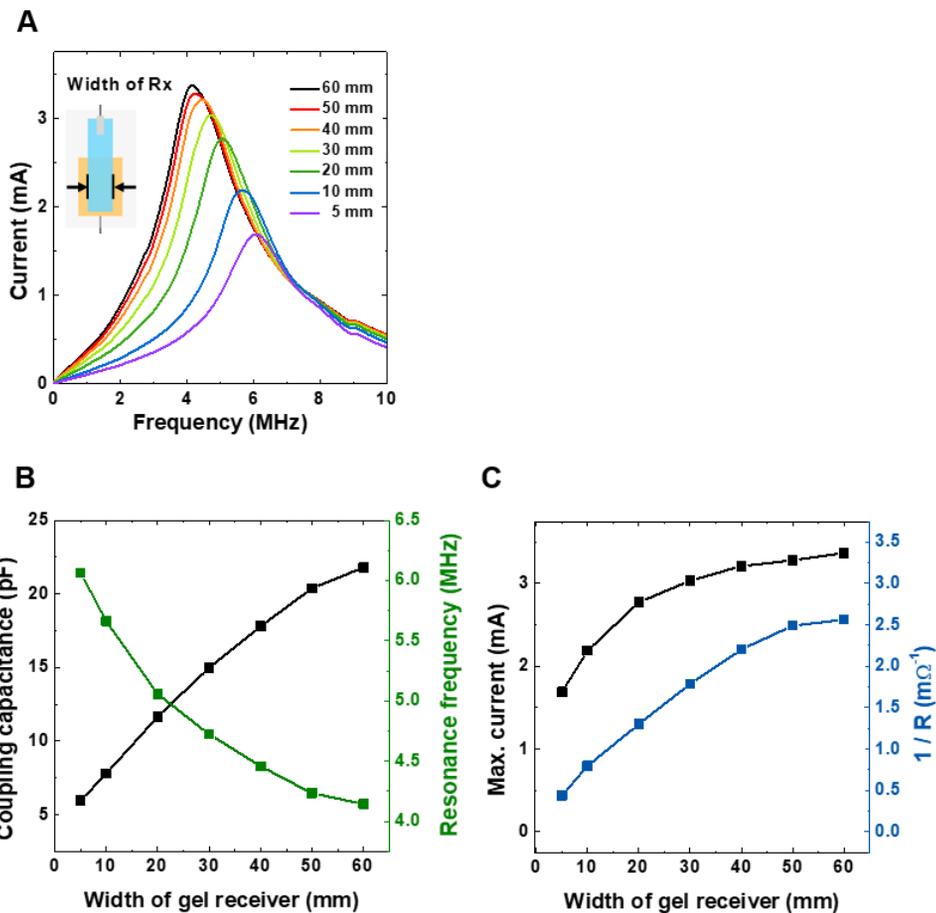
Fig. 3.9. (A) Currents measured at the receiver are shown as functions of frequency and the width of the gel receiver. The width of the gel receiver is related to the coupling area of the capacitor. The width of the transmitter was 50 mm. (B) The coupling capacitance was proportional to the width of the gel receiver and the resonance frequency was inversely proportional to the square root of the coupling capacitance. (C) Wide gel receivers delivered more current due to their larger cross-sectional area of the current path.

3.3.3 Implantation of an IWPT system.

In WPT systems, the gap between the transmitter and the receiver can be filled with a variety of materials, the properties of which directly affect the power transfer process. Generally, the capacitor gap is filled with a dielectric to enhance capacitance. However, for implantable applications, the capacitor gap can be filled with tissue and/or electrolytes having ionic conductivity. Thus, the performance of our IWPTs were examined as a function of the gap-filling material. The transmitter and receiver were covered with a thin insulator (Teflon tape, 80 μm) to avoid direct contact with the filler material. Fig. 3.10A shows the maximum current at resonance frequency as a function of gap distance with various materials. In air, the maximum current was reduced by half at a gap spacing of 15 mm. However, only a slight decrease was observed when the gap was filled with deionized water or NaCl solution. Since the impedance of the coupling capacitor is completely compensated by the inductor at resonance frequency, the current delivered at resonance frequency is maintained regardless of the coupling capacitance. With deionized water, the coupling capacitance was reduced from 94.9 pF (D = 15 mm) to 50.4 pF (D = 90 mm) with a constant current. The resonance frequency changed with the coupling capacitance (Figs. 3.10B and C). Note that air has a very low coupling capacitance (only 3.1 pF at D = 15 mm). Lower coupling capacitance induces a greater voltage across the coupling capacitor at resonance, which results in decreased efficiency [27, 28]. In contrast, the NaCl solution has a much larger capacitance (~ 220 pF) and no appreciable changes in coupling capacitance were observed as a function of gap distance. These differences result from the formation of different equivalent circuits constructed inside the respective coupling capacitor. When the capacitor gap is filled with a dielectric material, the equivalent circuit can be represented as shown in Fig.

89

3.11A. A dielectric capacitance (C_D) is generated by interactions between charges in the transmitter and ions in the gel receiver. The resistance of the gel receiver (R_{gel}) and an electrical double-layer capacitance (C_{EDL}) are connected in series with C_D. Thus, the total capacitance can be calculated according to Eq. (3.7),

$$\frac{1}{C} = \frac{1}{C_D} + \frac{1}{C_{EDL}} \approx \frac{1}{C_D} \tag{3.7}$$

where C_D varies with the capacitor gap, d_1. Conversely, C_{EDL} is fixed for a given interface and depends on the alignment of opposing charges over a few angstroms. Generally, C_D is much smaller than C_{EDL} ($C_D/C_{EDL} \sim 10^{-7}$) such that the total capacitance of the system is dominated by C_D. Therefore, overall capacitance decreases as the gap distance between the transmitter and the gel receiver increases. When the capacitor gap is filled with an ionic conductor, two capacitors, $C_D\#1$ and $C_D\#2$, are created across the thin insulator instead of C_D (Fig. 3.11B). The two capacitors are connected by R_{bulk}, which is determined largely by the concentration of ions in the bulk solution. R_{gel} and C_{EDL} are also connected in series with the other components. The total capacitance can therefore be derived using the following equation.

$$\frac{1}{C} = \frac{1}{C_D\#1} + \frac{1}{C_{EDL}} + \frac{1}{C_D\#2} \approx \frac{1}{C_D\#1} + \frac{1}{C_D\#2} \tag{3.8}$$

Note that the total capacitance is dominated by $C_D\#1$ and $C_D\#2$, which are much smaller than C_{EDL}. The total capacitance maintains a constant value regardless of the gap distance, d_3, because the separation distances between the two capacitors (d_2 and

90

d_4) are fixed according to the thickness of the insulator. As shown in Fig. 3.10A, when NaCl solution was used as the filler material instead of deionized water, the maximum current decreased slightly at low NaCl concentrations (0.01 M), and increased at high concentrations (0.1 M). This is because R_{bulk} varies with the concentration of electrolyte and the gap distance. Fig. 3.12 shows the total capacitance and series resistance between the transmitter and the receiver as a function of electrolyte concentration. C_D#1 and C_D#2 became charged with the ions immediately upon the addition of 0.001 M electrolyte. Since the capacitor is fully charged with only a small amount of ions, capacitance rose sharply to its maximum value at ion concentrations above 0.01 M. R_{bulk} is derived from ions in the bulk solution. A lack of bulk ions results in low conductivity and is evidenced by increasing series resistance. However, when delivering power through the skin, this effect is negligible because skin contains enough ions to maintain sufficient conductivity [29].

To demonstrate the operation of IWPT system in a body, the receiver unit was subcutaneously implanted in a mouse and powered transdermally. Fig. 3.13 shows the IWPT receiver unit, comprised of two gel receivers, a rectifier, and an LED, encapsulated in polydimethylsiloxane (PDMS) for implantation. The unit was implanted into a subcutaneous pocket and completely surrounded by skin and tissue (Fig. 3.14). A metal transmitter, insulated with Teflon tape, was placed on the skin where the receiver unit was inserted and a 50-MHz square wave was applied. Electrical power was transmitted through the skin to light the implanted LED (Fig. 3.15).
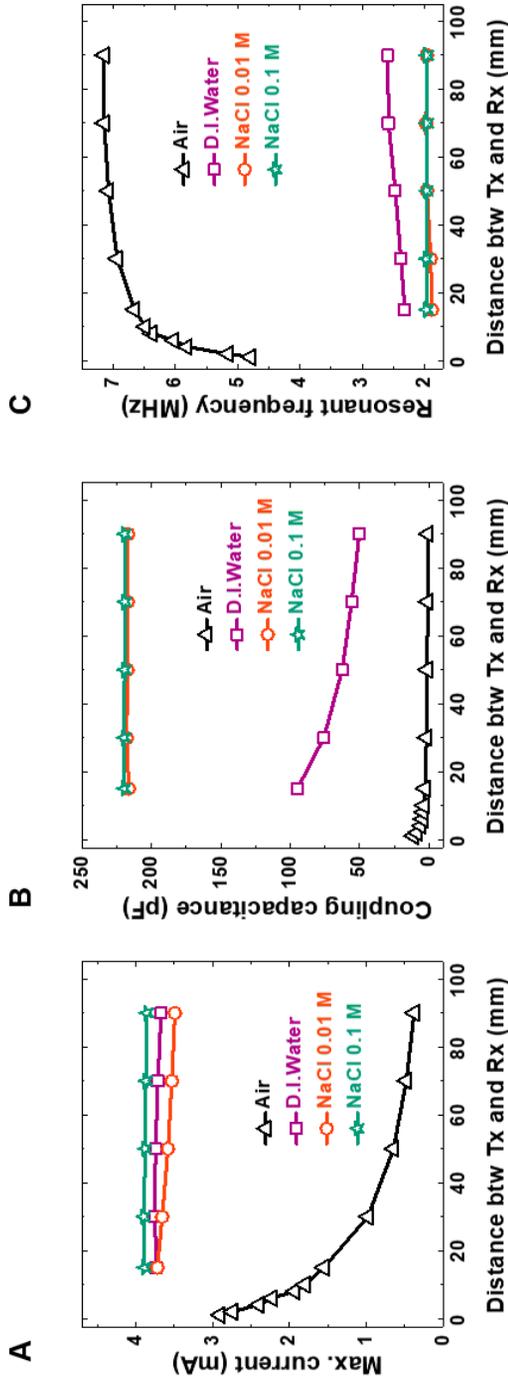
Fig. 3.10. (A) Maximum current is shown as a function of gap distance with various filling materials. (B and C) With dielectric materials such as air and deionized water, increasing the gap distance resulted in decreased coupling capacitance and increased resonance frequency. However, coupling capacitors filled with NaCl solution maintained a consistent coupling capacitance and resonance frequency regardless of gap distance.
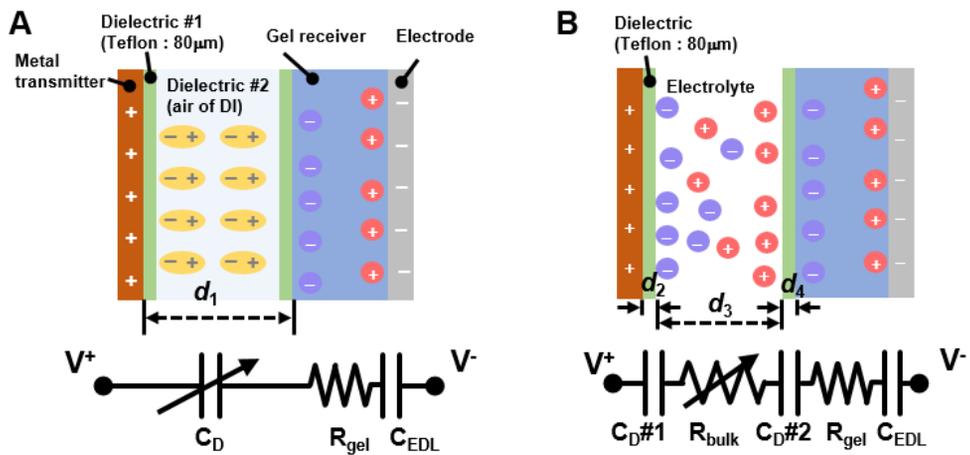
Fig. 3.11. (A) Schematic and an equivalent circuit illustrating a coupling capacitor filled with dielectric materials. C_D dominates the capacitance of the circuit and varies with gap distance. (B) Schematic and equivalent circuit illustrating a coupling capacitor filled with electrolyte. R_{bulk} is a variable resistance that changes with gap distance, while $C_D\#1$ and $C_D\#2$ were insensitive to gap distance.

Fig. 3.12. Coupling capacitance and series resistance of the coupling capacitor are shown as a function of electrolyte concentration. The lack of ions in the electrolyte solution increases R_{bulk} and results in decreased power transfer efficiency.

Fig. 3.13. An implantable IWPT device is shown. The gel receivers were encapsulated in polydimethylsiloxane (PDMS). The light-emitting diode (LED) was used as a load. The gel was dyed with Rhodamine B to increase visibility.
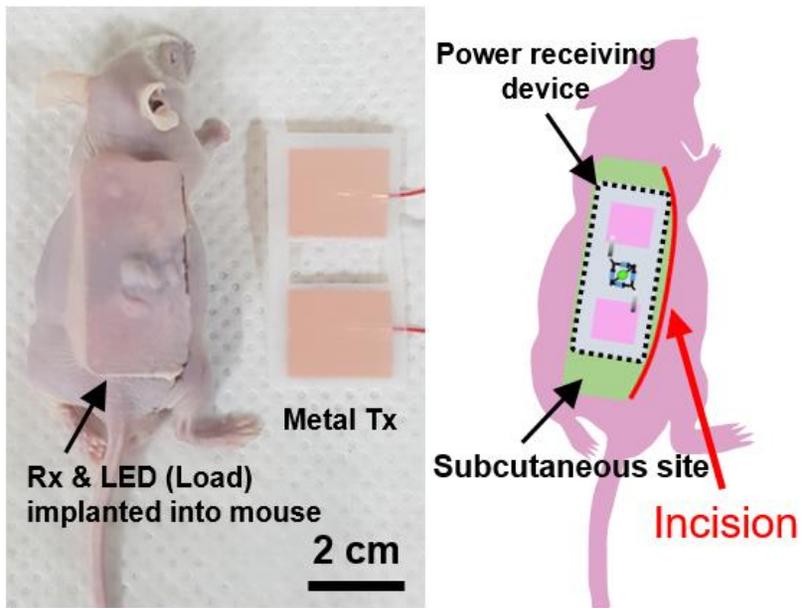
Fig. 3.14. This picture shows implantation of the IWPT device into a subcutaneous pocket in a mouse.
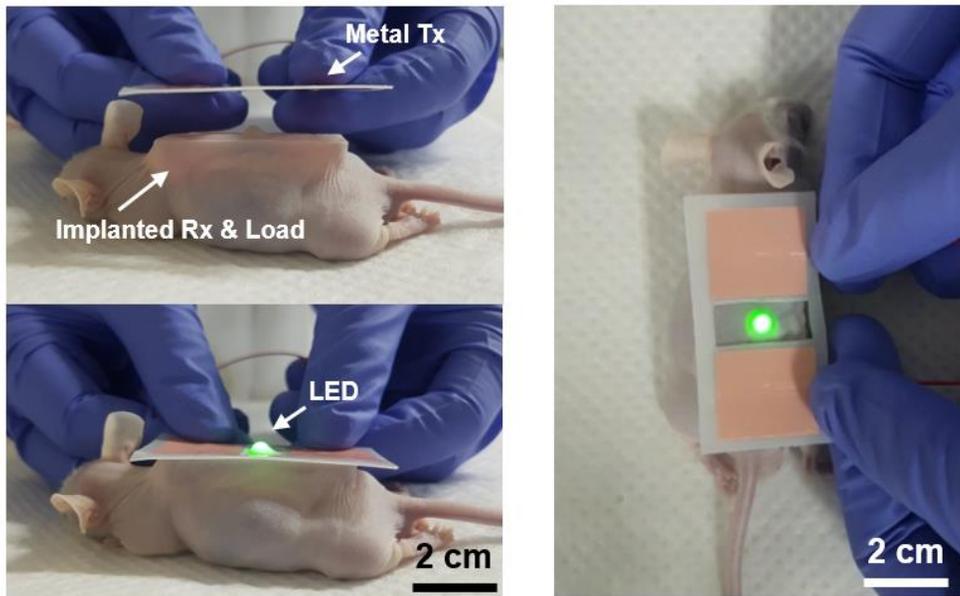
Fig. 3.15. Operation of the IWPT device after implantation in a mouse. When the transmitter was placed on the skin at the site of insertion, electrical power was transmitted through the skin to power the subcutaneous LED.

3.3.4 CAPDE for NADPH regeneration

While typically considered as undesirable side effects, the electrochemical reactions that occur in ionic devices can be a distinct advantage over electronic devices in that they can produce new compounds. In the previously discussed IWPT system, no electrochemical reaction occurs at the interface between the gel receiver and the electrode. For the electrochemical reaction to occur, voltage above certain range (~1V), so called the electrochemical window, must be applied to the C_{EDL}. Most of the voltage between transmitter and receiver is applied to the C_D so that the voltage across the electrical double layer, V_{EDL}, becomes less than 1 V. However, careful circuit design can raise V_{EDL} above the electrochemical window of the system, allowing electrochemical reactions through IWPT.

The schematic of an IWPT system for electrochemical reactions is illustrated in Fig. 3.16. Two gel receivers are connected by two diodes arranged in parallel, but with opposite directions. In this way, currents flowing into and out of the coupling capacitor are separated. Fig. 3.17A shows an equivalent circuit for electrochemical IWPT. Current flowing out of $C_{Coupling}$#1 passes through D#1, resulting in corresponding charge accumulation in C_{EDL}#1 and C_{EDL}#3. When the polarity of the source was changed, current flowing into $C_{Coupling}$#1 passes through D#2, allowing charges to accumulate in C_{EDL}#2 and C_{EDL}#4. The diodes prevent charges stored in the four C_{EDLS} to be discharged. If the current is continuously transmitted by the IWPT, then the voltage across the electrical double layer increases (Fig. 3.25). Fig. 3.17B shows a simulation of a voltage applied to the coupling and double layer capacitors. The inductance and coupling capacitance were set to 50 μH and 10 pF, respectively. An input signal ranging from of -10 to10 V was applied to the circuit. The voltage on the coupling capacitor is amplified by the LC resonance

and then decreases gradually as charges accumulate in the double layer capacitor. C_{EDL}#1 and C_{EDL}#2 are charged by opposing currents, resulting in voltages of opposite polarity. Since the voltage on C_{EDL} gradually increases and converges to the voltage of the input signal, an electrochemical reaction can occur if the input signal is larger than the electrochemical window.

IWPT system was then applied to generate electrochemical reactions for biochemical applications. Among the many electrochemically active biomolecules, NADPH was chosen because NADPH is a key reductant that drives numerous enzymes and helps control metabolism. An IWPT system for NADPH generation was designed as represented in Fig. 3.18. A polyacrylamide (PAAm) gel impregnated with $NADP^+$ in phosphate-buffered saline (PBS) buffer was used as the receiver. A working electrode (WE) was connected to the positive terminal of the diode and NADP reduction occurred at the interface between the WE and the gel ($NADP^+ + H^+ + 2e^- \rightarrow NADPH$, $E° = -320$ mV). A counter electrode (CE, Ag/AgCl) was connected to the negative terminal of the diode and oxidation occurred at the interface between the CE and the gel ($Ag + Cl^- \rightarrow AgCl + e^-$, $E° = 220$ mV). Based on these standard redox potentials, voltages over 540 mV were required to generate NADPH.

The gel receiver with $NADP^+$ was prepared with a width of 20 mm, length of 30 mm, and thickness of 2 mm. Titanium (Ti), which reportedly inhibits hydrogen evolution and promotes the synthesis of NADPH in the presence of $NADP^+$, was used as the WE [27]. The insulating layer between the WE and the receiver was 2 mm. The input AC signal of 10 $V_{peak-to-peak}$ (10 V_{pp}) was applied to the transmitter at the resonance frequency (6.2 MHz). The Faradaic current, generated by electrochemical reactions, was determined by measuring the voltage across the load (Fig. 3.19). Negligible current, and therefore negligible power transfer, was observed

in the absence of the gel receiver. The circuit was then evaluated with an NADP$^+$-impregnated gel receiver. Transmission of the input signal yielded a steady, rectified current with a maximum amplitude of 3.3 mA. The amplitude of the current output was linearly proportional to the amplitude of the applied voltage (Fig. 3.20) and decreased as the reaction continued.

The generation of NADPH was monitored optically by measuring fluorescence at 460 nm at an excitation wavelength of 340 nm. After 4 h of operation, an IWPT system consisting of a gel receiver containing 1 mM NADP$^+$ was irradiated at 365 nm and significant azure fluorescence was observed at the WE (Fig. 3.21). The boundary between the fluorescence volume and the bulk solution was blurry, indicating diffusion of NADPH inside the gel. To quantify the NADPH concentrations, absorbance was measured at multiple points within the interfacial volume around the WE using a NanoDrop 2000c ultraviolet-visible (UV-Vis) spectrophotometer. As shown in Fig. 3.22, gel absorbance at 340 nm appeared after initiation of the reaction and increased with reaction time. Notably, the absorbance began to decrease at reaction times exceeding 2 h and correlated with decreasing rectified voltage, as shown in Fig. 3.19. This decline in electrochemical activity may be attributed to the depletion of redox reactants, NADP$^+$ or Cl$^-$, in the gel. The influence of PBS concentration in the gel receiver on the generation of NADPH was also examined. IWPT performance was evaluated at PBS concentrations ranging from 10× to 0.01×, where 1× refers to a 0.01 M phosphate buffer and 0.154 M NaCl. Absorbance at 340 nm changed negligibly at PBS concentrations between 10× and 1×, but decreased significantly at lower concentrations (Fig. 3.23). Ions in the gel play an active role in power transmission and also partake in redox reactions. Thus, 10× PBS solution was used in subsequent experiments to ensure sufficient ion

concentrations.

The effects of the WE material on NADPH generation were also investigated by using WEs made of platinum (Pt), Ti, or stainless steel (SS), as shown in Fig. 3.24. NADPH concentrations were calculated based on the absorbance of the gel receiver at 340 nm and the reaction was allowed to continue for 2 h. The gel contained 1 mM $NADP^+$. Absorbance measurements were conducted at five different points within the interfacial area of the WE. Very little NADPH was produced at applied voltages less than 3 V_{pp}. On Pt and SS electrodes, NADPH was generated continuously as the applied potential was increased. In contrast, the Ti electrode yielded a maximum activity at 10 V_{pp}. It is likely that the cathodic reduction of water suppressed $NADP^+$ reduction. Previous studies on electrochemical NAD(P)H generation have shown that NAD(P)H reduction can be maximized by selecting a voltage that minimizes competing reactions. Our data show that the generation of NADPH on Ti was optimal at voltages less than 12 V_{pp}. Fig. 3.25 shows the amount of NADPH generated when a resistor was connected in parallel with the diode, creating a bypass circuit. The electrochemical reaction occurs only when current through C_{EDL} is blocked by the diode. With a bypass resistor in parallel with the diode, C_{EDL} is discharged by leakage current through the resistor, thereby lessening the ability of the circuit to drive electrochemical reactions. When a 1-kΩ resistor was connected in parallel with the diode, the gel absorbance decreased to a level similar to that of the pristine gel. The amount of NADPH generated was tunable depending on the value of the parallel bypass resistor.
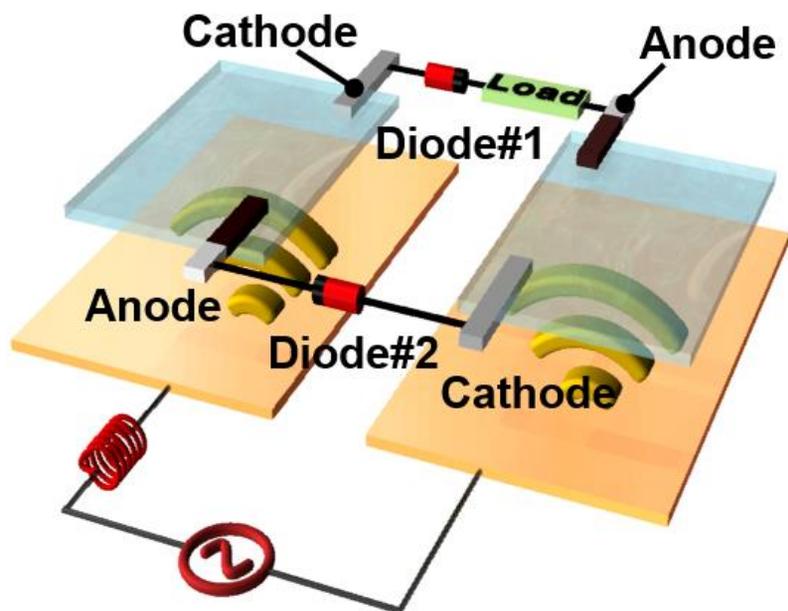
Fig. 3.16. A schematic of the CAPDE. Two receiving gels are connected by two diodes. A single diode lets the current flows only one way, so the second diode is required to serve a current returning path.
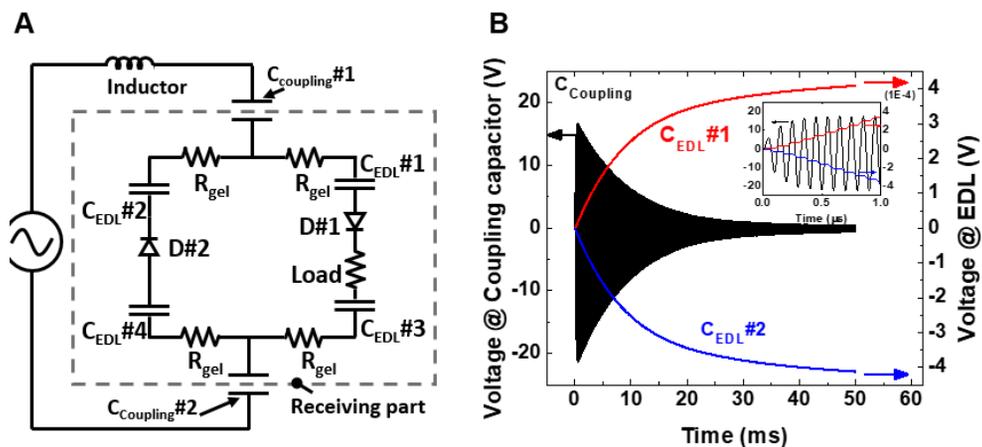
Fig. 3.17. (A) An equivalent circuit of the CAPDE. The two pair of Tx and Rx are represented by $C_{Coupling}$#1 and $C_{Coupling}$#2, and the interface between the gel receiver and the diode is represented by C_{EDL}. Four C_{EDL}s are generated at each interface. (B) Simulated voltages are shown on $C_{Coupling}$#1, C_{EDL}#1, and C_{EDL}#2. As current is transferred, $C_{Coupling}$#1 is repeatedly charged and discharged, while C_{EDL} is only charged due to the presence of the diode. As it is charged, the voltage on C_{EDL} increases gradually. An electrochemical reaction occurs when the voltage exceeds the electrochemical window.
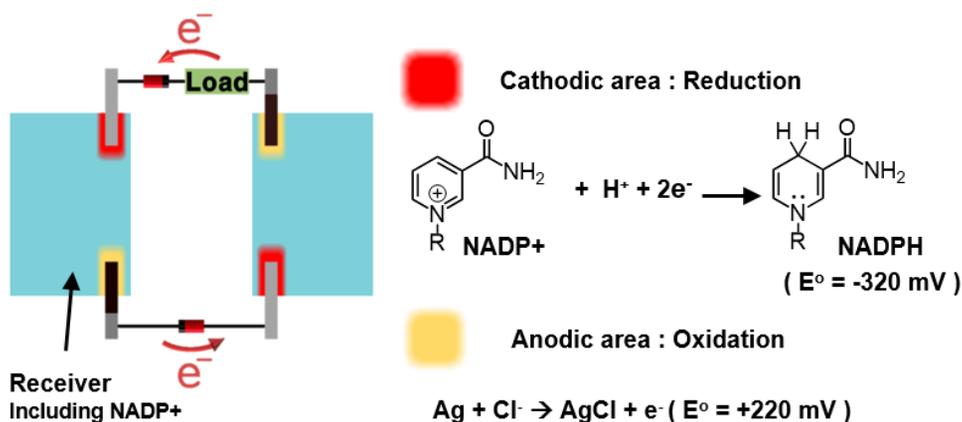
Fig. 3.18. The electrochemical generation of NADPH for an CAPDE system. The gel receiver contains 1 mM NADP+ and phosphate-buffered saline (PBS) buffer. The reduction of NADP$^+$ (NADP$^+$ + H$^+$ + 2e$^-$ → NADPH, E° = -320 mV) and the counter oxidation reaction (Ag + Cl$^-$ → AgCl + e$^-$, E° = 220 mV) occur at the working electrode (WE) and the counter electrode (CE), respectively. The products of electrochemical reactions accumulate at the interface between the gel receiver and the WE.
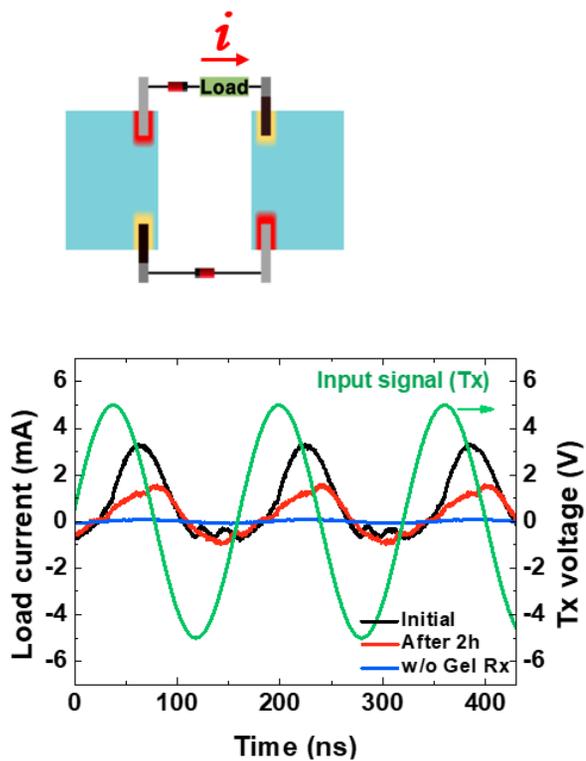
Fig. 3.19. The Faradaic current was determined by measuring the voltage across a 1-kΩ resistor on the receiver when subjected to a $10V_{pp}$ AC input. Measurements were obtained initially (black) and after 2 h of reaction (red), in the presence of 1 mM $NADP^+$ in the gel receiver and in the absence of a gel receiver (blue).
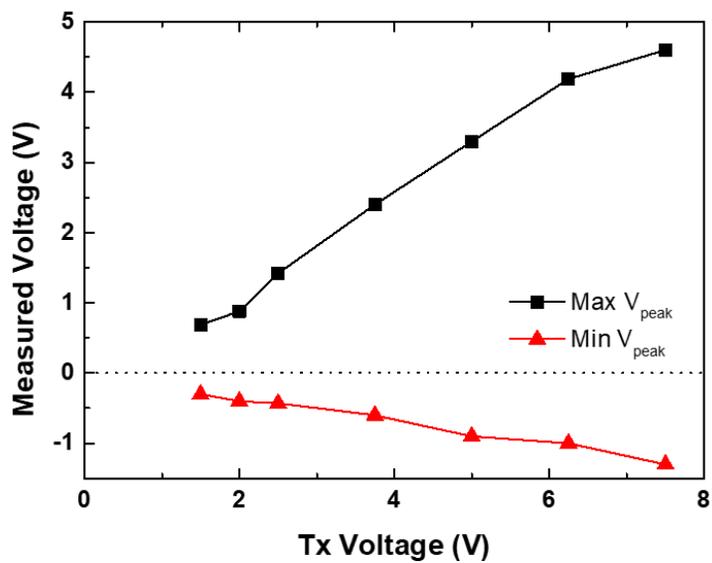
Fig. 3.20. The rectified alternating current (AC) voltage is shown for a gel receiver impregnated with 1 mM NADP$^+$. The circuit was operated with a Ti WE and the voltage was measured across a l-kΩ resistor between the WE and the CE. The maximum and minimum V$_{peak}$ values were recorded immediately after the input power was turned on.
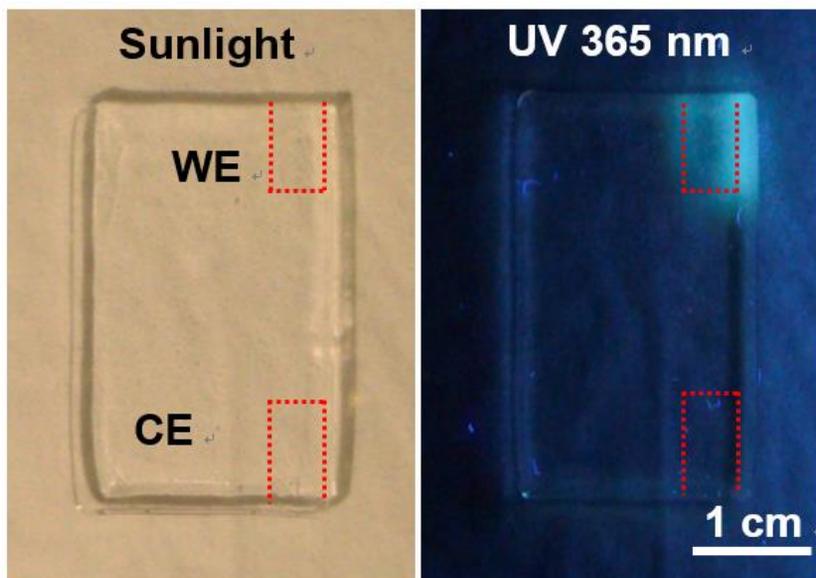
Fig. 3.21. Pictures of a gel receiver after 4 h of NADPH generation with a Ti WE under sunlight (left) and 365-nm light (right). The area immediately surrounding the WE showed azure fluorescence under ultraviolet (UV) illumination due to the synthesis of NADPH.
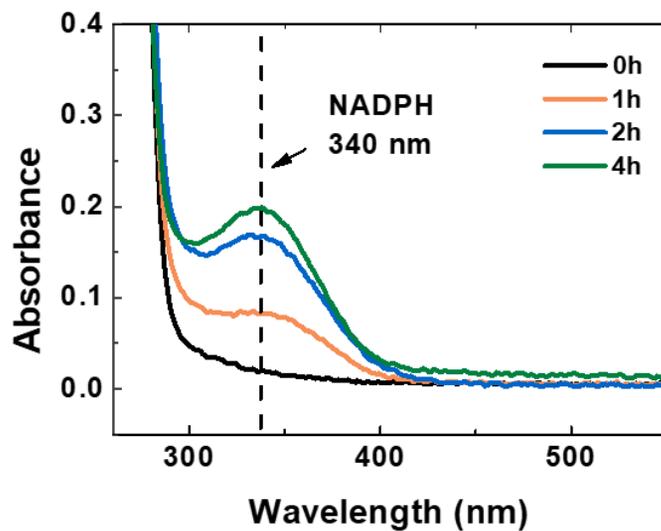
Fig. 3.22. The optical absorbance of the gel receiver at the WE was measured as a function of time to profile the NADPH concentrations. NADPH absorbs light at 340 nm, while NADP$^+$ does not absorb light in the vicinity of this wavelength.
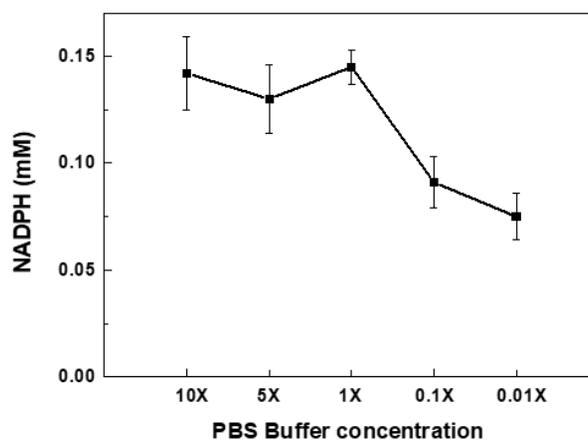
Fig. 3.23. The effects of PBS buffer concentration on the NADPH generation activity of a gel IWPT are shown. The NADPH generation reaction was conducted for 2 h with a gel containing 1 mM NADP+ and interfaced with a Ti WE.
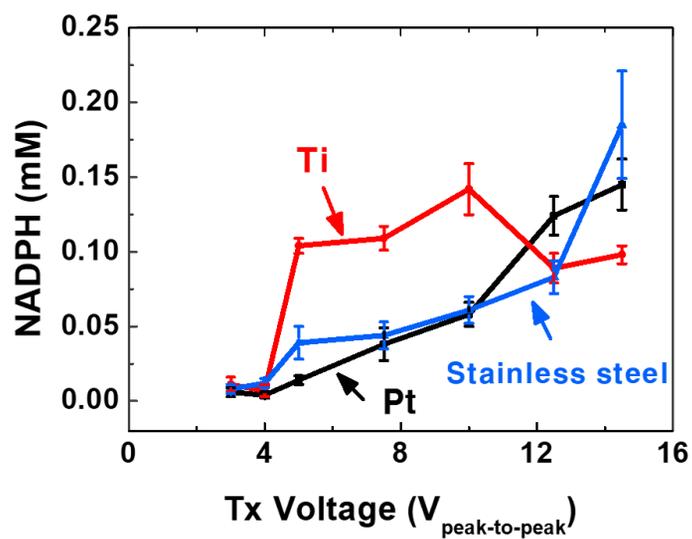
Fig. 3.24. The effects of different WE metals, i.e., platinum (Pt, black line), titanium (Ti, red line) and stainless steel (SS, blue line) on NADPH generation are shown.
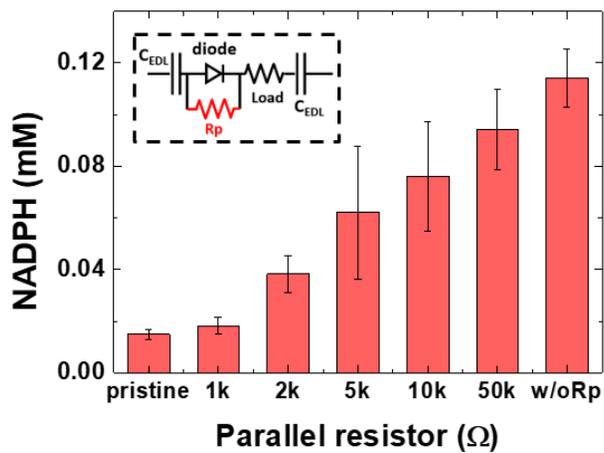
Fig. 3.25. The effects of a resistor connected in parallel with the diodes. The parallel resistor allows CEDL to be discharged, resulting in reduced electrochemical reactions.

3.3.5   Analysis of the voltages generated in the C_{EDL}

Analyses of the voltages generated in the C_{EDL} were performed using the simplified circuit shown in Fig. 3.26. Resistance components are omitted to exclude the effects of damping. The voltage across C_{EDL} increases beyond the electrochemical window because the diode blocks discharge of the charge stored in the C_{EDL}. The voltage across C_{EDL} continues to increase as the input signal is delivered. However, due to the high capacity of C_{EDL}, incremental changes in voltage due to charge delivery through one cycle of the input signal were small. Voltages beyond the electrochemical window occurred within a few milliseconds, because the input signal is transferred at a frequency of several MHz. The charge is stored alternately in C_{EDL}#1 and C_{EDL}#2 and the voltages across C_{EDL}#1 and C_{EDL}#2 follow the recurrence relationship shown below:

$$|V_{C,n}| = \frac{C_{Coupling}}{C_{Coupling} + C_{EDL}}\left(2V_s - \left(|V_{C,n-1}| + |V_{C,n-2}|\right)\right) + |V_{C,n-2}| \qquad (3.9)$$

where $V_{C,n}$ is the voltage across C_{EDL}, and n is the number of cycles. The first term on the right side indicates increasing voltage via charging. V_C converges to the amplitude of the source voltage, Vs.
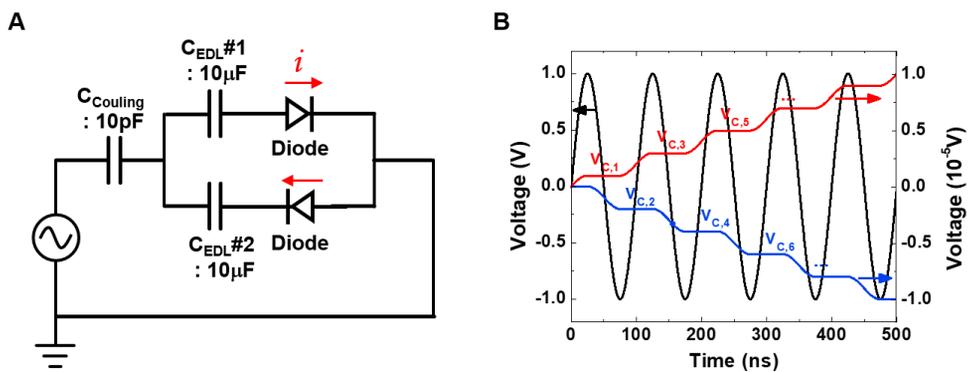
Fig. 3.26. (A) Simplified circuit diagram of IWPT for electrochemical reaction. (B) The voltage of the $C_{Coupling}$ (black), $C_{EDL}\#1$ (red), and $C_{EDL}\#2$ (blue) is simulated. Voltage of the $C_{EDL}\#1$ and $C_{EDL}\#2$ is increased by accumulated charges due to the diode.

3.4. Conclusion

We have demonstrated a WPT system incorporating an ionic conductor. Power was transferred through a coupling capacitor consisting of an ion conductive hydrogel receiver and a metal transmitter. Ionic currents, electrostatically induced by the time-varying electric field, could power the LEDs and charge the battery. To evaluate the capability of the IWPT as a power source for implantable devices, the IWPT was inserted to the subcutaneous site of the mouse and the power was transferred through the skin. IWPT is supposed to have no electrochemical reactions, but by controlling the flow of ions with the CAPDE, electrochemical reactions were generated at the interface between the receiving gel and the electrode. The electrochemically produced materials can be utilized to the biological systems. The NADPH, reducing agent in anabolism, was chosen as the target products and we could verify the generation of the NADPH.

Reference

[1]   Amar, Achraf Ben, Ammar B. Kouki, and Hung Cao. Power approaches for implantable medical devices. *sensors* **15**, 28889-28914 (2015)

[2]   Zabihian, A. R., et al. Implantable biomedical devices. Biomedical Engineering, Technical Applications in Medicine, *InTech, Rijeka,* 157-190 (2012)

[3]   Antonioli, G., Antonioli, G., Baggioni, F., Consiglio, F., Grassi, G., LeBrun, R., Zanardi, F., Stinulatore cardiaco impiantabile con nuova battaria a stato solido al litio. *Minerva Med* **64,** 2298-2305 (1973)

[4]   Agarwal, K., Jegadeesan, R., Guo, Y. X., Thakor, N. V, Wireless power transfer strategies for implantable bioelectronics. *IEEE reviews in biomedical engineering* **10,** 136-161(2017)

[5]   Xue, Rui-Feng, Kuang-Wei Cheng, and Minkyu Je. High-efficiency wireless power transfer for biomedical implants by optimal resonant load transformation. *IEEE Transactions on Circuits and Systems I* **60**, 867-874 (2012)

[6]   Kerzenmacher, S., Ducrée, J., Zengerle, R., & Von Stetten, F., Energy harvesting by implantable abiotically catalyzed glucose fuel cells. *Journal of Power Sources* **182,**.1-17 (2008)

[7]   Wang, Zhong Lin, Jinhui Song. Piezoelectric nanogenerators based on zinc oxide nanowire arrays. *Science* **312**, 242-246 (2006)

[8]   Xu, S., Qin, Y., Xu, C., Wei, Y., Yang, R., Wang, Z. L., Self-powered nanowire devices *Nature nanotechnology* **5**, 366 (2010)

[9]   Heetderks, William J. RF powering of millimeter-and submillimeter-sized neural prosthetic implants *IEEE Transactions on Biomedical Engineering* **35**, 323-327 (1988)

[10] Harrison, Reid R. Designing efficient inductive power links for implantable devices *2007 IEEE International Symposium on Circuits and Systems* (2007)

[11] Xu, S., Zhang, Y., Cho, J., Lee, J., Huang, X. *et al.*, Stretchable batteries with self-similar serpentine interconnects and integrated wireless recharging systems *Nature communications* **4, 1543** (2013)

[12] Zhang, Z., Alwen, A., Lyu, H., Liu, X., Li, Z., Xie, Z. *et al.* Stretchable transparent wireless charging coil fabricated by negative transfer printing *ACS applied materials & interfaces* **11**, 40677-40684 (2019)

[13] Koo, J., MacEwan, M. R., Kang, S. K., Won, S. M., Stephen, M. *et al.*, Wireless bioresorbable electronic system enables sustained nonpharmacological neuroregenerative therapy *Nature medicine* **24**, 1830 (2018)

[14] Boutry, C. M., Beker, L., Kaizawa, Y., Vassos, C., Tran, H., *et al.*, Biodegradable and flexible arterial-pulse sensor for the wireless monitoring of blood flow *Nature biomedical engineering* **3**, 47 (2019)

[15] Lu, Fei, Hua Zhang, and Chris Mi. A review on the recent development of capacitive wireless power transfer technology *Energies* **10**,.1752 (2017)

[16] Jegadeesan, R., Agarwal, K., Guo, Y. X., Yen, S. C., Thakor, N. V., Wireless power delivery to flexible subcutaneous implants using capacitive coupling *IEEE Transactions on Microwave Theory and Techniques* **65**, 280-292 (2016)

[17] Lee, Hae-Ryung, Chong-Chan Kim, Jeong-Yun Sun. Stretchable ionics–a promising candidate for upcoming wearable devices. *Advanced Materials* **30**, 1704403 (2018)

[18] Yang, Canhui, Zhigang Suo. Hydrogel ionotronics. *Nature Reviews Materials* **3**, 125 (2018)

[19] Koo, Hyung-Jun, and Orlin D. Velev. Ionic current devices—recent progress in the merging of electronic, microfluidic, and biomimetic structures

Biomicrofluidics **7**, 031501 (2013)

[20]   Keplinger, C., Sun, J. Y., Foo, C. C., Rothemund, P., Whitesides, G. M., Suo, Z., Stretchable, transparent, ionic conductors. *Science* **341**, 984-987 (2013)

[21]   Acome, E., Mitchell, S. K., Morrissey, T. G., Emmett, M. B., Benjamin, C. *et al.*, Hydraulically amplified self-healing electrostatic actuators with muscle-like performance *Science* **359**, 61-65 (2018)

[22]   Sun, J. Y., Keplinger, C., Whitesides, G. M., Suo, Z., Ionic skin *Advanced Materials* **26**, 7608-7614 (2014)

[23]   Kim, C. C., Lee, H. H., Oh, K. H., Sun, J. Y., Highly stretchable, transparent ionic touch panel. *Science* **353**, 682-687 (2016)

[24]   Sarwar, M. S., Dobashi, Y., Preston, C., Wyss, J. K., Mirabbasi, S., Madden, J. D. W., Bend, stretch, and touch: Locating a finger on an actively deformed transparent sensor array *Science advances* **3**, e1602200 (2017).

[25]   C. Larson, B. Peele1, S. Li, S. Robinson, M. Totaro, L. Beccai, B. Mazzolai, R. Shepherd, Highly stretchable electroluminescent skin for optical signaling and tactile sensing *Science* **351**, 1071-1074 (2016)

[26]   Lee, Y., Cha, S. H., Kim, Y. W., Choi, D., Sun, J. Y., Transparent and attachable ionic communicators based on self-cleanable triboelectric nanogenerators *Nature communications* **9**, 1804 (2018)

[27]   Theodoridis, Michael P. Effective capacitive power transfer *IEEE Transactions on Power Electronics* **27,** 4906-4913 (2012)

[28]   Mostafa, T., Bui, D., Muharam, A., Hattori, R., Hu, A., Capacitive Power Transfer System with Reduced Voltage Stress and Sensitivity *Applied Sciences* **8**, 1131 (2018)

[29]   Gabriel, C., A. Peyman, E. H. Grant. Electrical conductivity of tissue at frequencies below 1 MHz *Physics in medicine & biology* **54**, 4863 (2009)

[30]   Ali, Irshad, Tariq Khan, and Sasha Omanovic. Direct electrochemical

regeneration of the cofactor NADH on bare Ti, Ni, Co and Cd electrodes: the influence of electrode potential and electrode material. *Journal of Molecular Catalysis A: Chemical* **387** 86-91 (2014)

Chapter 4. Conclusion

In this dissertation, I have studied how to use hydrogel as a conductive material for ionic devices. Hydrogels are solid-like electrolytes that exhibit ionic conductivity similar to that of liquid electrolytes. Hydrogels are considered difficult to use in electronic devices, because they use ions as charge carriers instead of electrons. But this study shows that the hydrogels have sufficient conductivity to operate electronic devices while showing comparable signal transfer speeds to existing conductive materials. In addition, the unique properties of hydrogels, such as stretchability and transparency and biocompatibility, have enabled the ionic devices to overcome the limitations of existing electronic devices.

First, a highly stretchable and transparent ionic touch panel was demonstrated. A polyacrylamide hydrogel containing 2 M LiCl salts was used as an ionic conductor. The mechanism of position sensing in an ionic touch panel was investigated with a 1-dimensional strip. The ionic touch strip showed precise and fast touch sensing even with a highly stretched state. We expand the position sensing mechanism to a 2-dimensional panel. We could draw a figure using the 2-D ionic touch panel. The ionic touch panel could be operated under more than 1000 % areal strain. An epidermal touch panel was developed based on the ionic touch panel. The epidermal touch panel could be applied onto arbitrarily curved human skin, and its use was demonstrated by writing words and playing the piano and games.

. Second, we have demonstrated a new type of WPT system incorporating an ionic conductor. Electrical power was transferred through a coupling capacitor consisting of a metal transmitter and an ionic hydrogel receiver. Despite the high impedance of the capacitor due to its limited area, the efficiency of the IWPT was

enhanced by compensating the impedance of the capacitor with an LC resonance circuit. Our IWPT system was explored to evaluated the power transfer capability under the various conditions and supplied power to a subcutaneous device. The IWPT system was also used to generate NADPH, thereby demonstrating that IWPTs can be used to produce electrochemically active biomolecules. Although we focused on introducing the IWPT, the hydrogel is inherently stretchable material and can be easily designed to have bio-compatibility. It can be expected that the unique characteristic of hydrogel makes the IWPT more suitable for implant device supplying power into the body.

Abstract in Korean

유비쿼터스 컴퓨팅과 사물인터넷의 등장으로 사람과 기계간의 상호작용이 빈번해짐에 따라 휴먼-머신 인터페이스의 중요성이 점점 강조되어왔다. 휴먼-머신 인터페이스 기술의 발전에도 불구하고 금속과 반도체를 기반으로 한 현재의 디바이스들은 부드러운 피부와 조직을 가지고 있는 사람과의 기계적 물성의 불일치로 인해 사용이 제약되고 있다.

이런 측면에서 하이드로젤은 기존의 전도성 물질들의 대안으로서 등장했다. 하이드로젤은 다량의 수분을 머금고 있는 고분자 네트워크이다. 고분자 네트워크는 하이드로젤이 형체를 유지하고 또 변형을 견딜 수 있게 해주며 하이드로젤 내부의 수분은 이온을 녹여 하이드로젤이 이온 전도성을 가질 수 있게 해준다. 따라서 하이드로젤은 늘어난 상태에서도 전기 신호와 전력을 전달할 수 있는 신축성이 있는 전도체로 사용될 수 있다. 하지만 이온을 전하전달체로 사용한다는 것은 새로운 문제들을 야기할 수 있다. 이 논문에서 하이드로젤을 어떻게 이온 전도체로 이용하는지 또 그로 인한 문제들을 어떻게 다뤄야 하는지 말하고자 한다. 두 가지의 이온성 장치를 제작하였고 그에 대한 논의를 할 것이다.

첫 번째 장에서는 하이드로젤로 이루어진 투명하고 늘어날 수 있는 터치패널에 대해 논의할 것이다. 인간과 컴퓨터의 상호작용이 중요해짐에 따라 인간과의 통합이 가능하도록 생체적합성을 가지면서도

늘어날 수 있는 터치패널에 대한 수요가 증가하였다. 우리는 LiCl 염을 포함한 폴리아크릴아마이드 (polyacrylamide) 하이드로젤로 터치패널을 만들었다. 하이드로젤 터치패드는 부드럽고 신축성이 있어서 높은 변형을 견딜 수 있었다. 또한 하이드로젤은 높은 투명성을 가진 재료이기 때문에 가시광선 영역에서 98 %의 투명도를 보였다. 하이드로젤 터치패드는 표면 정전용량 식 터치 감지 시스템을 기반으로 제작되었으며 1000%가 넘는 변형이 주어진 상황에서도 정상적으로 작동하였다. 하이드로젤 터치패드는 피부에 부착된 형태로도 사용이 가능하였으며 피부에 부착된 상태로 글을 쓰거나 피아노를 치거나 게임을 하는 등의 동작을 수행할 수 있었다.

두 번째 장에서는 이온 전도체를 이용해서 무선으로 전력을 전달 할 수 있는 시스템에 대해 논의할 것이다. 이식형 의료장비에 전력을 제공할 수 있는 방법들 중에서 무선 전력 전송 방식은 지속적으로 충분한 양의 전력을 공급할 수 있다는 면에서 주목받고 있다. 대부분의 무선 전력 전송 시스템은 효율을 높이기 위해 전도성이 높은 금속을 사용하지만 금속은 딱딱하고 생체적합성이 부족한 재료이다. 이 논문에서 우리는 이온성 무선 전력 전송 장치를 제작하였다. 이온성 무선 전력 전송 장치는 부드럽고 투명하고 생체적합성이 뛰어난 하이드로젤 수신부를 통해 전력을 전달받는다. 이온성 무선 전력 전송 시스템은 5 cm 떨어진 거리에서도 전력을 전달 할 수 있었고 심지어 쥐의 피하에 이식된 전력 수신장치에도 피부를 통과하여 전력을 전달 할 수 있었다. 또한 이온성 장치에서 문제로 여겨지는 전기화학반응을

의도적으로 발생시키는 회로를 구성하여 원하는 전기화학반응을 유도해 낼 수 있었다. 이온성 무선 전력 전송 시스템 내에서의 전기화학반응의 발생 기작을 확인하였고 회로 설계를 통해 전기화학반응으로 인한 생성물의 양을 조절할 수 있었다.

Biography

Chong-Chan Kim

Building 30, Room 418, 1, Gwanak-ro, Gwanak-gu,
Seoul, 08826, Republic of Korea
https://scholar.google.co.kr/citations?hl=ko&user=HwIRCW0AAAAJ

EDUCATION & CAREER

Seoul National University   Seoul, Republic of Korea
Ph.D. in Materials Science & Engineering   Mar. 2014 - Feb. 2020

- Dissertation: A study on the ionic/electronic hybrid devices for touch sensing and wireless power transfer based on the soft hydrogels
- Committee: Ki Tae Nam (chair), Kyu Hwan Oh, and Jeong-Yun Sun

Seoul National University   Seoul, Republic of Korea
M.S. in Materials Science & Engineering   Mar. 2012 - Feb. 2014

Seoul National University   Seoul, Republic of Korea
B.S. in Materials Science & Engineering   Mar. 2007 - Feb. 2012

RESEARCH INTERESTS

- Developing soft machines using an ionic conductor
  - Measuring mechanical & electrical properties of the ionic conductor
  - Sensors: strain, pressure, temperature, touch, etc.
  - Actuators: dielectric elastomer actuators (DEAs), stimuli response actuators
  - Biocompatible devices
- Issues related to the gels served as an ionic conductor
  - Matter production control caused by electrochemical reactions at the interface
  - Circuit analysis involving impedance induced by electrical double layer

ONGOING WORKS

1. **<u>CC Kim</u>**, YH Kim, SH Jeong, KH Oh, KT Nam, JY Sun, "Ionic Wireless Power Transfer for biomedical devices", in preparation

PUBLICATIONS

1. **<u>CC Kim</u>**, HH Lee, KH Oh, JY Sun, "Highly stretchable, transparent ionic touch panel", Science 353 (6300), 682-687 (2016)

2. HR Lee, **<u>CC Kim</u> (Co-first Author)**, JY Sun, "Stretchable Ionics – A Promising Candidate for Upcoming Wearable Devices", Advanced Materials 30 (42), 1704406 (2018)

3. WS Cho, K Cho, JE Kim, TS Jang, EJ Ha, HS Kang, YJ Son, SH Choi, S Lee, **<u>CC Kim</u>**, JY Sun, HE Kim, "Zirconia-Polyurethane Aneurysm Clip", World neurosurgery 115, 14-23 (2018)

PATENTS

1. IONIC TOUCH PANEL
   A. Korea – Registration No. 10-1768648B1
   B. US – Application No. 16/321,090
   C. Europe – Application No. 17834628.4
   D. Japan – Application No. 2019-503251

PRESS RELEASE

Chong-Chan Kim et al. Stretchy, see-through touch panel made from salt-packed hydrogel.

- News on Chemical & Engineering News (Aug 22th, 2016)
  https://cen.acs.org/articles/94/i33/Stretchy-see-through-touch-panel.html
- News on phys.org (Aug 11th, 2016)
  https://phys.org/news/2016-08-gaming-stretchy-touchpad-video.html
- News on EurekAlert! (Aug 11th, 2016)
  https://www.eurekalert.org/pub_releases/2016-08/aaft-gua080816.php
- News on YTN science (Aug 12th, 2016)
  https://science.ytn.co.kr/program/program_view.php?s_mcd=0082&s_hcd=&key=201608121109038163&page=1574